Dear Dr. Hutchings,

Thanks very much to Thomas Armitage, the anonymous reviewer, and Harry Stern for their careful efforts to help improve our manuscript.

Below we reproduce all reviewers' comments in blue. We respond point-by-point in black text and report changes in indented quotes. At the end of this document is appended a "track changes" version of the revised manuscript.

Reviewer 1: Dr. Thomas Armitage.

The paper sets out a framework for estimating geophysical parameters relevant to the sea ice floe size distribution based on floe chord lengths measured by the CryoSat-2 radar altimeter. The paper exploits the fact that it is possible to distinguish between returns originating from leads and returns originating from floes, to estimate chord lengths as the distance over which consecutive CS2 waveforms are identified as floes uninterrupted by leads. These chord lengths are then related to the floe size distribution by statistical considerations. I was asked by the editor to assess the remote sensing aspect of this paper; I have not attempted to assess the theoretical developments because this is outside of my area of expertise, and I leave this to other reviewers. Based on the remote sensing aspect only, I would recommend publication after the authors address the following points.

P1 L8: radio should be radar

We corrected this typo! (pg 1, line 7)

> Applied to the CryoSat-2 radar altimetric record, covering the period from 2010-2018,

I would like to see a little more discussion on the limitations of the technique imposed by the sampling of the radar and its high sensitivity to areas of open water. Any amount of bright open water (lead) in the pulse limited footprint (300m along-track x 1.6km across-track) is likely to be identified as a lead or ambiguous. Also, bright open in the larger beam limited footprint (up to 20km across-track) can potentially lead to an ambiguous return (although this depends on the specific waveform processing). I think this could affect your processing in a few ways:

Thanks for bringing this to our attention.

Your assumption that theta is uniformly sampled: The fact that the altimeter footprint isnt symmetric means that for large theta the footprint is almost tangent to the floe perimeter when they intersect, whereas for small theta the footprint is almost perpendicular to the floe perimeter where they intercept. This means that chords with small theta are more susceptible to snagging or contamination by leads, particularly at the beginning and end of the chord closer to the floe edge. This means that the length of chords with small theta could be underestimated.

We agree chords with small θ are more susceptible to snagging for footprint orientations that are not entirely "floe". We amended Sec. 3 to read (pg 8, line 4):

> A chord length is taken from the midpoint of the first to the midpoint of the last radar echo. Individual chord lengths can be underestimated when continuous floes are separated artificially by producing two or more ambiguous echoes in sequence, or when highly reflective leads dominate the waveform return close to the floe edge and cause measurement dropout (Tilling et al., 2019). Lead contamination, or snagging (Armitage and Davidson, 2014) is more likely when the altimeter cuts of a small section of a floe, i.e. for small values of θ. Overestimates of chord length can also occur when ice floes are in close contact with neighboring floes. Therefore, floe chord lengths should be considered a satellite-derived product, not a true measurement of floe size. The minimum chord length retrieval D_{min} is limited to the CryoSat-2 footprint (300 meters along-track) (see the discussion in Appendix B).

In addition, in light of your comments and those of reviewer 2, we have amended the discussion of power law behavior in Section 4, with the analysis starting from a minimum scale $D_{min} = 900$ m (pg 10, line 9). This change did not substantially alter the results presented in the manuscript, for reasons discussed in the response to Dr. Stern below.

> We either (a) choose D^* to be 900 m (to reduce the impact of small-size sampling errors discussed in Sec. 2) or (b) use the scheme described in Clauset et al. (2007) to evaluate the most likely value of D^* for a power law tail.

2: Your taking Dmin as 300m (P8 L11): I think the minimum chord length (if you are taking a minimum of two consecutive floe measurements to represent the smallest possible chord) is closer to 600m. This is because for a waveform to be classified as a floe you really expect (at least) the pulse limited footprint to contain entirely sea ice and no open water any amount of open water will dominate the sea ice return. The other side of this is then that you can only assign a range to Dmin (from around 600m up to maybe 1200m if the leads either side are at the forward and backward limit of the along track footprints) and within this range it is ambiguous.

Thanks for pointing this out: we made a typo in describing how a single chord was identified. We now explain (pg 8, line 3):

> Floe chords are defined as a continuous sequence of one or more floe echoes, with a gap of one ambiguous echo permitted within a floe sequence to allow for anomalous returns.

and (pg 8, line 12),

> However, surface discrimination via altimetry is highly accurate in months without melt ponds, (Peacock and Laxon, 2004; Guerreiro et al., 2017; Quartly et al., 2019), giving confidence that floe echos represent a coherent length of ice. More details on the details of chord identification may be found in Tilling et al. (2019).

As mentioned above, we additionally no longer use D_{min} to classify the power-law behavior across all scales, instead using a more conservative 900 m: (pg 10, line 9),

> We either (a) choose D^* to be 900 m (to reduce the impact of small-size sampling errors

discussed in Sec. 2) or (b) use the scheme described in Clauset et al. (2007) to evaluate the most likely value of D^* for a power law tail.

Figure 3 and P9 L3-10: You claim that the largest representative radii lie along the Canadian Archipelago, but the maps show that the largest radii actually surround the pole hole.

(NB: We broke this paragraph up). Thanks, we now changed how we described the region of largest sizes: (pg 9, line 27),

> The largest representative radii in the Arctic lie in the interior Arctic near the pole, with a tongue of large floes that extends along the Canadian Arctic in late winter.

and (pg 14, line 34),

> Geographic variability of representative radius is broadly similar between model and observation: the largest floes lie in the Arctic interior, with regions of smaller floes in the straits and continental margins.

It seems like there is a geophysical signal, with larger radii in the MYI zone, which I would expect, but then superimposed on that is a signal that seems to increase with latitude such that the largest floe sizes are close to the pole hole. I was wondering if you have an explanation for the large floe radii surrounding the pole hole, because this isnt something I would intuitively expect? The spatial sampling increases as you move north due to the convergence of orbits, could this skew the mean floe radius large?

We added a supplementary figure to discuss this: while indeed the representative floe size does increase with latitude, there is not a covariance between floe size and the number of chord measurements. We discuss in the text (pg 9, line 28):

> There is a notable increase of representative radius with latitude. In the Supporting Info Fig. S2, we show that this relationship cannot be explained as a result of the increasing density of measurements near the pole and may therefore be a geophysical signal.

as well as in the Supporting Info, Text S3

> Fig. S2(a) shows the relationship between annual-average representative radius and latitude in the Arctic, which demonstrates a rapid increase above 80°N. Fig. S2(b) shows the relationship between annual-average representative radius and the number of observed chord lengths. There is a weak covariance of the number of chords and representative radius, and therefore we the increase in (a) is not a result of the higher pass density near the pole.

Incidentally I couldnt find Figure S1?

We responded to the reviewer comment with the missing figure and have included it in the new

revision.

Reviewer 2

We thank the second reviewer for their efforts in improving our work.

General comments: This paper aims at developing a new method to obtaining the floe size distribution in the Arctic Ocean using the chord length data derived from the CryoSat-2 altimeter data. The conversion of the chord length distribution to floe size distribution statistically seems to the highlight of this paper. The authors accomplished this with a strong mathematical background and an assumption of circular shapes of ice floes and homogeneous and isotropic distribution. With this method, they attempted to show the geographical, seasonal, and interannual properties of the floe size distribution in the Arctic Ocean for the first time. They also tested the validity of power law distribution which has been applied for the floe size distribution frequently. As a result, they concluded that although power law scaling cannot be ruled out, the statistical basis is limited and especially the assumption of power law is weak in the Chukchi and Beaufort seas. They also emphasized the refinement of this method for the operational use.

Floe size distribution is one of the important parameters of sea ice and should be considered to understand the behavior of sea ice area. However, due to the limited observations, its statistical properties are not clarified yet. The idea of using the chord length is interesting in that it can cover wide areas and the truncation error caused by the traditional analysis of finite area seems to be reduced. Therefore, I agree this paper presented an interesting and useful method to analyze the floe size distribution. But to do so, I think the new method should be validated carefully with observational data and the consistency should be confirmed by comparing it with the traditional method. This paper focuses mainly on the availability of the new method with their strong mathematical background. While I feel this is an important step, the validation of this method seems relatively weak. In this case, I think the validation is especially important because their method is based on several assumptions such as circular shapes or homogeneous distribution. Thus, while I agree their method is interesting, my evaluation for this paper is somewhat reserved. In addition, the descriptions are not necessarily readable at places for me, and might be improved, I feel. The major points are as follows:

We thank the reviewer for their careful reading and for placing our study in context of the existing literature. A technically complete validative study is indeed something necessary to pursue, but not within the scope of this study which is to lay out this concept and how it is applied. We explain (pg 3, line 5):

> To date, however, these studies have not been designed to facilitate a comparison with model data, nor have altimetric studies been used to compile floe size statistics. These objectives are the focus of this work.

and (pg 3, line 11):

> One of the key aims of the paper is to develop floe size distribution measurements that are useful for model validation and calibration.

and in the conclusions (pg 17, line 20):

> This paper has focused on the framework for making altimetric measurements of the FSD and comparison to model output, but the obtained chord lengths and distributions have not been carefully validated against other observational methods, and this will be necessary before further application of this method.

1) Assumptions of this method. The authors assume that the floe chord distribution data is homogeneous, isotropic, and stationary within the region, and time data is collected (P3L17-18). For simplicity in mathematical treatment, it might be allowed. But I think the validity of these assumptions should be examined somewhere in the paper. For example, fracture patterns caused by shear stress near the shore are far away from circular shapes (e.g., Schulson and Hibler, 1991 Journal of Glaciology). As a preliminary step, I encourage the authors to confirm this method is available even in such situation based on the real floe patterns. Besides, to make an assumption of stationary distribution, the time scale on which this assumption is valid should be discussed because they discuss the seasonal and interannual variation of FSD later. If they examined that their method is applicable to obtain floe size distribution by comparing with the traditional analysis based on real satellite images, the value of this paper would have been enhanced significantly.

We now explain that the timescale of stationarity assumed in this manuscript is one month (pg 9, line 5):

> The full CryoSat-2 dataset examined here spans the time period from October 2010 to November 2018, and floe chords measured using the above technique are binned into the CICE sea ice model's two-dimensional sea ice grid for each month and year to facilitate comparison with model products. This implies that the principles of isotropy, homogeneity and stationarity of the FCD, required to produce such a distribution, are invoked on the length scale of the CICE model grid and time scale of a month.

And discuss the issue of different fracture patterns and their impact on statistics on pg 4, line 24,

> Nevertheless, it will likely be necessary to amend the analysis below in the future to account for more realistic shape distributions and geometries (e.g., diamonds (Wilchinsky and Feltham, 2006)), regional differences in floe shape properties (such as in regions where shear stress determines ice shape (Schulson and Hibler, 1991)), or to evaluate the sensitivity of the results that follow to the assumed shape distribution.

Theoretical support with mathematics is important, but that is not enough, I think.

This perspective is widely shared by the authors. Far more work is required before this method can be operationally applied to geophysical problems. However, performing a full validation study first requires a theory to validate, and we hope to perform this important work in the coming future.

2) Technical matters To represent floe size, they used a radius of the equivalent circle (P3L7). Is it common? To my knowledge, a diameter has usually been used in the past studies. I think a diameter fits the sense of floe size better, although this might be an essential matter.

We now cite the use of the "effective radius" (pg 3, line 19):

> Define a floes size, r, as its "effective radius" — the square root of the floe's area divided by π (Rothrock and Thorndike, 1984; Horvat and Tziperman, 2015)) We use radius instead of diameter, as appears in some other observational studies, for comparison with model output in Sec. 5

In the past studies, floe size distribution has been represented in two ways: cumulative number distribution and non-cumulative one. To avoid confusion, it might be better to declare which way this paper takes somewhere in section 2.

We explain the FSD is non-cumulative now when defining the FSD in Sec. 2 (pg 3, line 31),

> In the same region, we define the (non-cumulative) number FSD $P(r)$, where $P(r)dr$ is the fractional number of floes with a size between r and $r + dr$ in A, and is also normalized to one.

In section 3, how they determined the individual chord lengths from the Cryosat-2 records is still unclear to me. When ice floes are contacting the neighboring floes, how did they determine the boundary? How much is the measurement accuracy of vertical distance? If it is about 10 cm, it would be quite difficult to identify the edge of the floe for thin ice especially. I think this is a critical matter.

We agree that the measurement of floe boundaries is complicated, as highlighted in the response to Reviewer 1. We now add further clarity in Sec. 3 (pg 8, line 5):

> Individual chord lengths can be underestimated when continuous floes are separated artificially by producing two or more ambiguous echoes in sequence, or when highly reflective leads dominate the waveform return close to the floe edge and cause measurement dropout (Tilling et al., 2019). Lead contamination, or snagging (Armitage and Davidson, 2014) is more likely when the altimeter cuts of a small section of a floe, i.e. for small values of θ. Overestimates of chord length can also occur when ice floes are in close contact with neighboring floes.

And discuss challenges in regions of thin ice in the Discussion (pg 17, line 27):

> The assumption of scale-invariant sampling, observational uncertainty because of the finite sampling resolution, analysis of ambiguous returns, and the accuracy of retrievals in regions of thin sea ice may also affect the inferred size of sea ice floes. This in turn may affect the climatologies described in this study.

In section 4, they tested the validity of power-law distribution. It might be possible that the real FSD may have different regimes although the power-law is applicable for each regime. Figure 4 may suggest such possibility. In such a case, how do they judge the validity?

We explain why we do not consider multiple regimes now (pg 12, line 1):

> We note that a "power law" describes the scaling of a distribution's tail. Previous observational studies have discussed "double power laws" (i.e., Toyota et al., 2011), i.e. two power-law distributions of different exponent joined at a specified scale. The methods employed here would capably capture the large-size power law scaling but not the small-scale scaling. Such "double power laws" are necessarily scale-variant, and require at least 3 parameters to describe. The conceptual and mathematical simplicity of the "power law hypothesis" does not apply in such a case, and we do not consider them here.

Interpretation of the results Overall, I feel the discussion of the results might be a bit weak compared with the preparatory statement about mathematical treatment. For example, they showed During the months of October-December, the climatological representative radius is roughly 35% larger than February-April (P8L32-34). I would like to know how they interpret this result because from intuition floe size tends to become larger at the later growth stage. I am wondering if the measurement accuracy might affect this result significantly.

Thanks, we now explain (pg 9, line 19):

> We interpret this seasonal cycle in size over time as due to the formation of large first-year ice pans in October which are later fractured into smaller floes throughout the winter months

And discuss measurement accuracy in the discussion (pg 17, line 27):

> The assumption of scale-invariant sampling, observational uncertainty because of the finite sampling resolution, analysis of ambiguous returns, and the accuracy of retrievals in regions of thin sea ice may also affect the inferred size of sea ice floes. This in turn may affect the climatologies described in this study.

4) The applications of the results They examined the validity of power-law distribution (section 4) and the application to numerical sea ice models (section 5). But since the validity of this method is not fully investigated from the observations, I am wondering if these applications might be really useful. Especially, it was difficult for me to understand the authors intention about section 5. Personally, at this stage I prefer focusing on showing the validity of this new method to extending the results to models.

We explain the motivation for Sec. 5 in the introduction (pg 3, line 5),

> To date, however, these studies have not been designed to facilitate a comparison with model data, nor have altimetric studies been used to compile floe size statistics. These objectives are the focus of this work. ...
> One of the key aims of the paper is to develop floe size distribution measurements that are useful for model validation and calibration. In Sec. 5, we show a proof-of-concept,

> demonstrating how altimetric data can be used to constrain and evaluate new models of the FSD, comparing the CryoSat-2 FSD data to a climate model simulation with a prognostic FSTD model.

how it may be useful even in the presence of such uncertainty (pg 17, line 33),

> Yet observational uncertainties regarding, for example, the floe shape distribution can be roughly estimated at the order of the error in "effective radius" obtained for circular floes ($r = \sqrt{A/\pi}$) or a square ($r = \sqrt{A/4}$), a relative error of 25%. To constrain model results beyond this scale of error will require further refinement. However, as shown in Fig. 6, at present the model-data mismatch in the interior Arctic can exceed a factor of 3. Even with expected levels of error in the present derived FCD/FSD product, some constraints on the model can be considered at present with this method.

and explain the need for validation on pg 17, line 33:

> The positive comparison between model and observation in Section 5 could also be due to a compensation between these measurement uncertainties and will need to be re-examined in future validation work.

Specific comments: (P1L2) spare should be replaced by sparse.

Thanks!

(P1L15) covered in sea ice might be covered with sea ice.

Thanks!

(P1L18, P2L12) Rothrock and Thorndike, 1984b I could not see the difference between 1984a and 1984b in the reference lists. If they are the same, please take b.

Indeed there was none, we have fixed!

(P2L19-20) This is true. But to describe this, it would be needed to show that FCD is better than FSD in accuracy.

We would appreciate that this comment be clarified, perhaps the page number is incorrect? We did edit this sentence as follows (pg 2, line 21):

> Improvements in the quality and quantity of available FSD data are needed before arriving at consensus derived FSD statistics to guide and assess model performance.

(P3L15) the fraction of floe chords should be the number fraction of floe chords?

Yes, thanks!

> For a domain of horizontal area A, and over a period of time ΔT that corresponds to several repeat satellite passes, we bin the set of recorded floe chords to form a probability distribution $S(D)$, which we term the "floe chord distribution" (FCD), where $S(D)dD$ is equal to the number fraction of floe chords in A over ΔT with length between D and $D + dD$, and is normalized to one.

(P3L3) In Eq.1, F(r;D) S(D) can be replaced by F(r;D) S(D) dD dr to show the number of floes which have radius between r and r+dr. The same applies for the righthand term.

This is true, but for simplicity we hope it is ok to not add differentials to both sides. See the next comment where we improved out explanation of the equation following your comments.

(P3L24) I wonder if F(r;D) dr dD should be F(r;D) S(D) dr dD. (P3L27) Likewise, I wonder if F(D;r) dr dD should be F(D;r) P (r) dr dD.

We have rearranged the sentence to make this more clear (pg 4, line 5)"

> The conditional probability $F(r; D)$ relates given chord lengths to the floe size distribution that could generate them: $F(r; D)dr$ is the probability that floes with size in the range from r to $r + dR$ were sampled given a chords of length D. The conditional probability $\tilde{F}(D; r)$ relates given floe sizes to the chord length distribution they generate: $\tilde{F}(D; r)dD$ is the probability of measuring a floe chord of length from D to $D + dD$ given that a floe of size r was measured.

(P4L1) D/r should be from 0 to 2 (not 1).

Thanks! We had defined ξ incorrectly in the text:

> where $G(\xi) = G(\frac{D}{2r})$ is an unknown function that integrates to 1 over the interval from $\xi = 0$ to 1.

(P5L1) I wonder that since they consider a circle rather than a semi-circle, theta should take between 0 and 2*pi (not pi).

We explain now (pg 5, line 1):

> Because of rotational symmetry, we need only consider $\theta \in [0, \pi)$, sampled according to a probability distribution $T(\theta; r) = \pi^{-1}$.

(P5L1) Please state the definition of the function T.

We do now (pg 5, line 1):

> Because of rotational symmetry, we need only consider $\theta \in [0, \pi)$, sampled according to

a probability distribution $T(\theta; r) = \pi^{-1}$.

*(P6L18) Please insert under the condition, alpha ¿ n+1 after explicitly.

We do now (pg 7, line 6):

Moments of a power-law tail can be evaluated explicitly (for $\alpha > n + 1$),

(P6L23) In Eq.13, I wonder if e (epsilon) should be 1-e.

Thanks for catching this, we wrote the definition of $R_{n,\epsilon}$ incorrectly, - we fix now (pg 7, line 7):

Then for both the FCD and FSD, the ratio of two moments is independent of the unknown coefficient C, i.e.,

$$R_{n,\epsilon} \equiv \frac{\langle D^{n+\epsilon-1} \rangle}{\langle D^{n-1} \rangle} = D_{min}^{\epsilon} \frac{n - \alpha}{n + \epsilon - \alpha}, \tag{1}$$

valid for $n + \epsilon < \alpha$. The power-law coefficient can be obtained for any n, ϵ as,

$$\alpha_{n,\epsilon} = n + \epsilon \frac{R_n}{R_n - D_{min}^{\epsilon}} = \text{ constant.} \tag{2}$$

(P7L5-12) Sorry, but I could not follow this paragraph. It would be helpful if you rewrite this paragraph with an emphasis of your intention.

We rewrote this paragraph (pg 7, line 18):

If the power law hypothesis holds, then the two estimates of α agree, although the aggrement of $\hat{\alpha}$ and $\alpha_{n,\epsilon}$ is not sufficient to confirm the power-law hypothesis. In the Supporting Information (Text S1 and File S1), we include Matlab code that compares the two estimates, and shows that they agree even for small ($N < 25$) sets of power-law distributed data. While in practice Eq 13 is easy to apply, it only holds when $\alpha_{n,\epsilon} > n + 1$, and unlike the method of Clauset et al. (2009), it does not allow for a robust statistical analysis of the power-law fit, and should only be used when the data is assumed to follow a power-law already.

(P9L5-6) This sentence may contain grammatical error. Please rewrite it.

We rewrote this sentence (pg 9, line 25):

We display only those areas with at least 25 recorded floe lengths in each month during the averaging period. In Supporting Information Text S2 and Fig S1, we examine the sensitivity of bulk FSD statistics to this threshold, finding similar seasonal cycles and climatologies.

(P9L9) representative radius from fall and spring might be representative radius between fall and spring.

Thanks! (pg 9, line 32):

> The difference in representative radius between fall and spring is accounted for by the reduction of floe sizes in regions near the Arctic interior (see Fig. 6).

(P11L11-13) I could not understand this sentence.

We re-wrote this sentence (pg 11, line 10):

> We use $M = 10,000$, which permits computation of p within 0.005 (Clauset et al., 2009), and rule out the power-law hypothesis under the condition $p < 0.1$ (Virkar and Clauset, 2014).

(P12L4-5) Assuming: : : parameterizations. is hard to follow.

We re-wrote this paragraph (pg 12, line 27):

> Sea ice parameterizations that assume a power law distribution may significantly bias sea ice statistics. The imposition of any fixed distributional shape, when FSD dynamics are scale-variant, leads to implicit non-local redistribution of sea ice between floe size categories (Horvat and Tziperman, 2017). To see this in practice we compare the difference in Arctic-wide representative radius, $\overline{r}$, which is used in parameterizations of wave attenuation and ice thermodynamics, between the most-likely power-law fit to the data and the "true" value obtained via Eq. 6. The observations yield $\overline{r}$ =10.2 km, versus 34.5 km for the power-law fit. Examining only the tail of the distribution (chord lengths above 24.7 km) yields better agreement: 23.7 km for the observations and 24.4 for the fit line. Yet this tail constitutes just 1% of all measured chord lengths, corresponding to just 18% of total ice area and 4.5% of the perimeter per square meter (Eq. 7).

(P13L16) The two: : : hypothesis. I could not understand why.

We rewrote this sentence to be more clear (pg 14, line 4):

> The two estimates disagree — as their agreement is necessary for the power law hypothesis to be true (see Sec. 4, SI Text S1), this alone is sufficient to rule it out.

(P13L29) below 300 m should be below 30 m. Please check Steeles paper. Accordingly, necessitating a maximum floe size of 1 km should be reconsidered.

We now state (pg 14, line 21):

> Previously published model runs (Roach et al., 2018) focused on the impact of the FSD on lateral melt, which is largely driven by small floes (Steele, 1992), and so floe sizes above 1 km were not considered.

(P16L19-20) Floe size modeling efforts have focused on the marginal ice zone I think some citation is needed.

We changed this to "marginal ice zone processes" and added citation here (pg 17, line 14):

> Floe size modeling efforts have focused on marginal ice zone processes (Horvat and Tziperman, 2015; Zhang et al., 2015), and particularly floe sizes below about 1 km because these small floes play an important role in sea ice thermodynamics for floe sizes.

(P16L30) I could not understand the meaning of structural uncertainty.

We changed this to "observational uncertainty" (pg 17, line 27):

> The assumption of scale-invariant sampling, and observational uncertainty because of the finite sampling resolution, may also affect the inferred size of sea ice floes.

Short Comment: Harry Stern

Hi Chris, Good idea to use satellite altimeter data to look at sea-ice floe chord lengths, which are related to floe sizes. This allows an Arctic-wide analysis over several years, which has not been done. Here are my (unsolicited) comments, in the nick of time (discussion closes tomorrow)!

Harry, thanks very much for taking the time to add your comments here.

Main Comments

You reference Rothrock and Thorndike (1984) (R&T hereafter) in several places, which is very appropriate, since that is the fundamental paper on measuring the sea ice floe size distribution. However, you did not give credit to R&T for the concept of the chord length distribution and its close relationship to the floe size distribution (FSD). This is from the Abstract of R&T: Another sampling strategy is to measure the lengths of line segments on floes. The distribution of these chord lengths is equivalent to the distribution of floe diameters. Furthermore, there is an entire section in R&T called Chord Length Distribution in which its relationship to the FSD is derived. Look at R&T equation (4):

Now look at your equation (9). The similarity in form, together with the meaning of the variables, must be more than chance. Surely R&T were onto something very similar to what you did. Not to take away from your theoretical development, which possibly goes beyond R&T, but please give proper credit to the originators and developers of the connection between chord length and FSD.

We appreciate greatly this being brought to our attention — we were (at least consciously) ignorant of the referenced section, but this connection between floe sizes and chords of circular floes was investigated previously, both by R&T and others. We added text to explain this fact (pg 2, line 34):

> One-dimensional measurements of sea ice properties, like along-track altimetric measurements of ice open water, have long been sought to describe the two-dimensional ice surface. Rothrock and Thorndike (1984) originally described a method for reconstructing the sea ice floe size distribution in a region using straight-line measurements over the geometry of floes. Lindsay and Rothrock (1995) later compiled the statistics of lead and ice spacings in two-dimensional imagery. Other work has taken place to derive and understanding the width distribution of individual leads in visual imagery and altimetry (Wadhams et al., 1988; Key and Peckham, 1991; Key, 1993; Wernecke and Kaleschke, 2015), which can be used to estimating heat fluxes and turbulent transfer between the ocean and atmosphere. To date, however, these studies have not been designed to facilitate a comparison with model data, nor have altimetric studies been used to compile floe size statistics. These objectives are the focus of this work.

2. In the Abstract, you state: we produce the first climatology and seasonal cycle of sea ice floe size statistics. However, two previous works also produced a seasonal cycle of floe size statistics, namely Perovich and Jones (2014), which you cite in a different context, and Stern, HL,

Schweiger, AJ, Stark, M, Zhang, J, Steele, M and Hwang, B. 2018. Seasonal evolution of the sea-ice floe size distribution in the Beaufort and Chukchi seas. Elem Sci Anth, 6: 48. DOI: https://doi.org/10.1525/elementa.305 See Figure 8 in Stern et al.

This is a good point, and we should have been more specific. We now change the abstract to state (pg 1 line 7):

> Applied to the CryoSat-2 radar altimetric record, covering the period from 2010-2018, and incorporating 11 million individual floe samples, we produce the first pan-Arctic climatology and seasonal cycle of sea ice floe size statistics.

And in the introduction we explain (pg 2, line 11):

> The observational record of floe statistics derives from visual imagery localized in space and time (i.e., Rothrock and Thorndike, 1984; Toyota et al., 2006; Steer et al., 2008; Toyota et al., 2011) or from repeat measurements in the same region over multiple months (Hwang et al., 2017; Stern et al., 2018a), which may subsequently used to compile a seasonal cycle of the FSD (Perovich and Jones, 2014; Stern et al., 2018a).

3. First paragraph of Section 3 (top of page 8): CryoSat-2 radar echo returns have approximately a constant along-track spacing of 300 meters; floe chords are defined as a continuous sequence of two or more floe echoes; and single isolated floe returns are eliminated. Therefore it seems to me that the shortest chords must be 600 meters long. Yet the paper states in multiple places that the analysis applies down to 300 meters. How is that possible?

As discussed in the response to Dr. Armitage, the "floe chord" dataset includes single echos, and we clarify (pg 8, line 3):

> Floe chords are defined as a continuous sequence of one or more floe echoes, with a gap of one ambiguous echo is permitted within a floe sequence to allow for anomalous returns

As you state on page 5 (lines 18-19), the representative radius can represent only those floes whose size is larger than rmin, the smallest possible floe size sampled. Agreed. Furthermore, it seems to me that the representative radius is actually proportional to rmin. If rmin is halved, the representative radius is halved. So I dont really understand the use of a representative radius, e.g. as depicted in Figure 3, unless its to look for changes over time. The absolute value of the representative radius is simply a reflection of the resolution of CryoSat-2; it doesnt seem to have an intrinsic meaning. The vast majority of floes in the Arctic are smaller than rmin.

The described relationship between representative radius and r_{min} holds under the power-law assumption, with $f(r)$ decaying uniformly and algebraically from r_{min} to infinity. Since we record distributions that have finite maximum values for r and are not power laws, this is not the case: indeed preliminary results from the ICESAT-2 altimeter indicate slightly *larger* floe sizes with a higher resolution. We explain in the text now (pg 6, line 5):

These derived quantities are useful because they require no further information about the sea ice (such as its concentration) to compare against modeled FSDs. However, both $\overline{r}$ and $\mathcal{P}$ can represent only those floes whose size is larger than $r_{min} = D_{min}/2$, the smallest possible floe size sampled. For perfect power-law distributions beginning at a scale of r_{min} or before, both metrics are functions of r_{min}. However, for the real FCDs measured here, a maximum floe size exists, and a power-law scaling is not found approaching r_{min}, so the use of such metrics is justified (see Sec. 4).

This sensitivity did inform our decision to not produce maps of $\mathcal{P}$, and so we add (pg 6, line 16):

However, because $\mathcal{P}$ is a proportional to a negative moment of the FCD, it is sensitive to changes in the number of small chord lengths. Because of the measurement uncertainty for smaller chord lengths we will focus instead on $\overline{r}$ which is instead a positive moment of the FCD.

Minor Comments

Page 5, equation (3). The inequality r ¡ D/2 is backwards. It should be r ¿ D/2.

Thanks! We fixed this inequality.

Page 5, line 10. For the beta function, use the letter B instead of the Greek , and state that B is the beta function, because this is the first place where it appears in the paper.

Indeed, we now state (pg 7, line 3):

$$A_n \equiv \int_0^1 \xi^n G(\xi) d\xi = \frac{2^{n+1}}{\pi} \int_0^{\frac{\pi}{2}} \sin(x)^n dx = \frac{2^n}{\pi} B\left(\frac{n+1}{2}, \frac{1}{2}\right),$$

where B is the beta function.

Page 6, line 10. I dont understand what is meant by where we leverage that because it is a probability distribution... What is being leveraged?

We re-write this (pg 6, line 23):

where the integral of the left-hand side of Eq. 1 is equal to $S(D)$ as $\int F(r; D)dr = 1$

Page 6, equation (13). Rn is not defined. Is it the same thing as Rn, of equation (12)?

Thanks! This equation is now (pg 7, line 7):

$$\alpha_{n,\epsilon} = n + \epsilon \frac{R_{n,\epsilon}}{R_{n,\epsilon} - D^{\epsilon}_{min}} = \text{ constant.} \tag{3}$$

Page 7, Figure 2. (i) In panel (d), the label on the x-axis says Spacing (m) but it should be kilometers (km). (ii) In panel (d), its impossible to tell which tick mark corresponds to 1 km. Please use short tick marks for unlabeled values and long tick marks for labeled values. (iii) The caption says that the satellite track is from January 21, 2014, but the text (page 8, line 17) says January 14, 2018.

Thanks for these edits - we moved the hashes to the plot to avoid this confusion and changed the labeling (see new Fig 2).

Page 8, line 17. Check date, compare to Fig 2 caption.

We fixed this date in the text (pg 9, line 1):

> Figure 2 shows an example of floe chord data for a single CryoSat-2 track over the Arctic on January 21, 2014.

Page 8, line 19. Should red circle be blue circle?

Indeed it should - thanks!

Page 10, Figure 4. (i) I dont understand p in this figure. Panel (a) has three curves, two of which have p=0. Panel (b) has three curves, one with p=0 and one with p=5. The caption refers to p ¡ 0.1 and p ¿ 0.1. What is p? (ii) The x-axes of panels (a) and (b) are labeled m (meters?) but should probably be km. (iii) The caption (line 3) refers to equation 11 but should probably be equation 13 or 14. (iv) I dont understand the shading in panels (a) and (b). The caption says that the gray (or blue) shading is the difference between the blue and black curves. But where the blue and black curves cross, the difference should be zero, but the shading doesnt reflect that.

We altered the legend, fixed the axis labeling and equation, cleared some of the clutter in the image, and eliminated the confusing p-values in the legend. The caption reads (Fig 4, caption):

> Examining the power-law hypothesis. (a) Histogram of all chord lengths recorded in the Arctic for the months November-April (black). Bin centers indicated by hashes and are logarithmically spaced. Blue line is power-law fit to all observed sizes according to eq. 14. Red line is power-law fit to the tail. Dashed red lines are fit lines using the $\pm$ 1 standard deviation values of $\hat{\alpha}$. Red vertical line is the most likely beginning of the power law tail, D^*, with shaded region $\pm$ 1 standard deviation in D^*. (b) Same as (a), but for measurements in April.

Page 11, the MLE method, and Appendix C. You might mention that the MLE method was also recommended and applied by Stern et al. (2018) (On reconciling disparate studies...): see their Section 5.1 for a summary. Your Appendix C through equation C5 is essentially the same as Stern

et al. Appendix A.

Indeed! We now better explain that many studies have been suggesting/deriving/using this method (pg 10, line 5):

> This method has been used to evaluate power-law behavior in recent FSD model Horvat and Tziperman (2017) and observational studies Hwang et al. (2017); Stern et al. (2018b) and proceeds as follows:

During the derivation we now state (pg 21, line 1):

> Following (Muniruzzaman, 1957; Clauset et al., 2009) (see also the derivation in Stern et al. (2018a)),

Page 11, line 16. The range from 300 m to 100 km is not 3 orders of magnitude, its 2.5. Also, if the smallest chords are in fact 600 m long (see Main Comment #3) then the range would be 2.2 orders of magnitude.

We eliminated the "order of magnitude" statement (pg 12, line 6):

> To illustrate why this is important, we first consider the entire set of 11 million chord lengths recorded in the Arctic in all months (October-April), spanning a length range from 300 m to 100 km.

Page 13, lines 18-21. There is a seasonal cycle in the steepness of the distributional tail: shallowest in early winter and steeper in late winter... the changes across the winter months may be due to a reduction of the largest floes... These observations are similar to the ones made by Stern et al. (2018) (Seasonal evolution of...), e.g. in the Abstract: The mean power-law exponent goes through a seasonal cycle... consistent with the processes of floe break-up in spring followed by preferential melting of smaller floes in summer and the return of larger floes after fall freeze-up. You might add a sentence comparing your results to those of Stern et al.

We do so now (pg 14, line 10):

> A similar seasonal cycle to that found in Fig. 6(a,c), with an FSD that steepens from September to April, was found in image analysis of floes in the Beaufort and Chukchi Seas (Stern et al., 2018b), with $\alpha \approx 2.5$, although the distribution steepened monotonically over that period.

Page 13, line 30. Change resolve to resolved
Page 15, line 8. Change Straits to straits (lower case)

Thanks!

Page 16, line 3. Id suggest changing global to Arctic-wide or pan-Arctic. Also, the use of the phrase

high-resolution here is highly questionable. Stern et al. (2018) catalogued 18 studies of the FSD. Fifteen of them used higher-resolution data than this study.

Agreed - we made these changes (pg 16, line 30):

> This method provides the first pan-Arctic accounting of climate-relevant quantities derived from the FSD, permits testing of existing scaling laws previously used to characterize distributions of floe size, and allows for gridded comparisons between FSD models and observations.

Page 16, line 6. Again, I dont think 3 orders of magnitude is accurate.

Fixed this (pg 16, line 32):

> Using this new technique we produced climatological, annual-average, and geographic mean moments of the Arctic FSD across a range of resolved length scales from 300 m to 100 km.

Page 20, line 4. This sentence doesnt make sense. It should say something like: Take the derivative of L with respect to and set the result equal to zero to arrive at (equation C4).

Thanks - we add now (pg 21, line 5):

> As the natural log is monotonically increasing in its argument, to find the most likely α, denoted $\hat{\alpha}$, we take the derivative with respect to α and solve a similar equation,

Page 20, line 15. There is no C in Appendix A. Perhaps it should say Equation 10.

We re-organized and re-wrote this material (pg 21, line 10):

> The above analysis concerns the most likely α that explains the FCD. We may ask a separate question: what is the most-likely α, which we define as α_P, that would explain the FSD, given the explicit relationship that can be derived between $S(D)$ and a power-law distributed $P(r)$ examined in Eq. 10:

Page 20, equation C9. The final summation is missing the natural logarithm function, i.e. it should be the sum over ln (Di/D*).

Thanks, fixed!

Page 20, line 22. ...that lie below D*. should this be above D*?

We removed this sentence from the revised manuscript.

Page 21, line 4. Change least to at least

Fixed, thanks!

Page 21, line 10. Either change radii to radius or delete the word a before representative.

Thanks! (pg 22, line 10).

> Nearly all regions where wave fracture is an active process also have representative radii below about 10 km (Roach et al., 2019)

Page 24, Rothrock and Thorndike (1984) is listed twice.

Thanks! This has been fixed.

Estimating The Sea Ice Floe Size Distribution Using Satellite Altimetry: Theory, Climatology, and Model Comparison

Christopher Horvat[a], Lettie Roach[b,c], Rachel Tilling[d,e], Cecilia Bitz[f], Baylor Fox-Kemper[a], Colin Guider[g], Kaitlin Hill[h], Andy Ridout[i], and Andrew Shepherd[j]

[a]Institute at Brown for Environment and Society, Providence, RI, USA
[b]National Institute for Water and Atmospheric Research, Wellington, NZ
[c]Victoria University of Wellington, Wellington, NZ
[d]Cryospheric Sciences Laboratory, NASA Goddard Space Flight Center, Greenbelt, MD, USA
[e]Earth System Science Interdisciplinary Center, University of Maryland, College Park, MD, USA
[f]University of Washington, Seattle, WA, USA
[g]University of North Carolina, Chapel Hill, NC, USA
[h]University of Minnesota, Minneapolis, MN, USA
[i]Center for Polar Observation and Modelling, University College London, London, UK
[j]Center for Polar Observation and Modelling, University of Leeds, Leeds, UK

Correspondence: Christopher Horvat (horvat@brown.edu)

Abstract. In sea-ice-covered areas, the sea ice floe size distribution (FSD) plays an important role in many processes affecting the coupled sea-ice-ocean-atmosphere system. Observations of the FSD are ~~spare~~ sparse — traditionally taken via a painstaking analysis of ice surface photography — and the seasonal and inter-annual evolution of floe size regionally and globally is largely unknown. Frequently, measured FSDs are assessed using a single number, the scaling exponent of the closest power law fit to the observed floe size data, although in the absence of adequate datasets there have been limited tests of this "power-law hypothesis". Here we derive and explain a mathematical technique for deriving statistics of the sea ice FSD from polar-orbiting altimeters, satellites with sub-daily return times to polar regions with high along-track resolutions. Applied to the CryoSat-2 ~~radio~~ radar altimetric record, covering the period from 2010-2018, and incorporating 11 million individual floe samples, we produce the first pan-Arctic climatology and seasonal cycle of sea ice floe size statistics. We then perform the first pan-Arctic test of the power law hypothesis, finding limited support in the range of floe sizes typically analyzed in photographic observational studies. We compare the seasonal variability in observed floe size to fully coupled climate model simulations including a prognostic floe size and thickness distribution and coupled wave model, finding good agreement in regions where modeled ocean surface waves cause sea ice fracture.

1 Introduction

Earth's polar oceans are covered ~~in~~ with sea ice: a thin, heterogeneous interface that plays an important role in the coupling between ocean and atmosphere. Sea ice is a collection of many individual pieces, called floes, which may be characterized in terms of a horizontal length scale, their "size". On the large scales relevant to global climate modeling, the statistical variability of floe

size is described using the floe size distribution ~~(FSD, Rothrock and Thorndike, 1984b)~~(FSD, Rothrock and Thorndike, 1984a) .

The FSD is an important property of the sea ice cover that influences the multiscale temporal and geographic variability of sea ice, akin to the grain size in sedimentology or particle size distribution in atmospheric chemistry. The scale of individual floes plays a role in many sea-ice-related processes: sea ice melt rate (Steele, 1992; Horvat and Tziperman, 2017, 2018), the evolution of the oceanic mixed layer (Manucharyan and Thompson, 2017), atmospheric boundary layer exchange (Birnbaum and Lüpkes, 2002; Lüpkes and Birnbaum, 2005; Tsamados et al., 2014), the sea ice response to applied stress (Feltham, 2008; Wilchinsky and Feltham, 2011), and the propagation of waves into the ice (Squire et al., 1995; Squire, 2007; Smith and Thomson, 2016). The importance of the sea ice FSD has led to the development of diagnostic FSD models of varying complexity ~~(Williams et al., 2013; Zhang et al., 2016; Bateson et al., 2019)~~(Williams et al., 2013; Zhang et al., 2015; Bateson et al., 2019) , and a prognostic floe size and thickness distribution (FSTD) scheme (Horvat and Tziperman, 2015; Roach et al., 2018a).

Despite the potential relevance of sea ice floe size to polar climate evolution, there remain no climate-scale assessments of average floe size or the FSD. The observational record of floe statistics derives from visual imagery localized in space and time ~~(i.e., Rothrock and Thorndike, 1984b; Toyota et al., 2006; Steer et al., 2008; Toyota et al., 2011) or~~ (i.e., Rothrock and Thorndike, 1984a; ~~or from~~ repeat measurements in the same region over ~~several months (Hwang et al., 2017; Stern et al., 2018b)~~multiple months (Hwang et al., 2017; Stern et al., 2018a), which may subsequently used to compile a seasonal cycle of the FSD (Perovich and Jones, 2014; S . FSD measurements are obtained by identifying individual floes within a 2-dimensional image of the sea-ice surface. Because floe sizes span several orders of magnitude, accurate representations of the FSD — even in relatively small geographical domains and in perfect lighting and surface conditions — require high resolution and high observational coverage. Nearly all measurements of the FSD have been made in accordance with a “power law" scaling hypothesis commonly used to describe multiscale systems (Mandelbrot and Wheeler, 1983), in which the resulting FSD is fit to a straight line in logarithmic coordinates, whose slope, α, is reported as an intrinsic property of the floe mosaic. There is large uncertainty in these scaling coefficients, the range they apply over, and their applicability and origin (Herman, 2011; Horvat and Tziperman, 2017; Herman et al., 2018; Stern et al., 2018b). Improvements in the quality and quantity of available FSD data are needed before arriving at consensus derived FSD statistics to guide and assess model performance.

Here we ~~describe~~ outline a method that exploits satellite radar altimetry to construct the FSD and its moments across polar regions with sub-kilometer spatial resolution, sub-daily temporal resolution, and spanning multiple orders of magnitude in size. Altimeters, like the ones carried on the Envisat, ICESat, CryoSat-2, and ICESat-2 satellites, make repeated, frequent passes over polar oceans, and substantial efforts have been made to process the satellite returns to discriminate between open water, floes, and leads. The altimetric returns have found many uses, including reconstructing the sea ice thickness field (Laxon et al., 2013; Tilling et al., 2016, 2018b) and ocean surface circulation under sea ice (Peacock and Laxon, 2004; Armitage et al., 2018). Fields inferred from altimetry have led to advances in understanding polar systems: from forecast and climate prediction (Day et al., 2014) to model validation (Schröder et al., 2018; Allard et al., 2018) to climate change studies ~~(?Kwok, 2018)~~ (Laxon et al., 2003; Kwok, 2018), and have been evaluated and validated using field campaign data (Skourup et al., 2017; Sandberg Sorensen et al., 2018; Tilling et al., 2018b).

One-dimensional measurements of sea ice properties, like along-track altimetric measurements of ice open water, have long been sought to describe the two-dimensional ice surface. Rothrock and Thorndike (1984a) originally described a method for reconstructing the sea ice floe size distribution in a region using straight-line measurements over the geometry of floes. Lindsay and Rothrock (1995) later compiled the statistics of lead and ice spacings in two-dimensional imagery. Other work has taken place to derive and understanding the width distribution of individual leads in visual imagery and altimetry (Wadhams et al., 1988; Key , which can be used to estimating heat fluxes and turbulent transfer between the ocean and atmosphere. To date, however, these studies have not been designed to facilitate a comparison with model data, nor have altimetric studies been used to compile floe size statistics. These objectives are the focus of this work.

We outline the mathematical theory that allows for comparing altimetric datasets and the FSD in Sec. 2. In Sec. 3 we apply this method to a new dataset of segmented CryoSat-2 sea ice type data from 2010-2018. Using this data we produce the first climatological maps of mean sea ice floe size and fragmentation for the Arctic Ocean. We then test the power law hypothesis, finding limited support for power-law scaling across most of the dataset in Sec. 4. One of the key aims of the paper is to develop floe size distribution measurements that are useful for model validation and calibration. In Sec. 5, we ~~examine~~ show a proof-of-concept, demonstrating how altimetric data can be used ~~in model comparison and improvement~~to constrain and evaluate new models of the FSD, comparing the CryoSat-2 FSD data to a climate model simulation with a prognostic FSTD model. We conclude in Sec. 6.

2 Floe Chords and the Floe Size Distribution

For an individual pass over sea ice by a polar-orbiting satellite altimeter, return waveforms along the satellite orbit track are assigned a surface type depending on the waveform shape and coincident sea ice concentration (Tilling et al., 2018b). A “floe chord" of length D is a continuous series of points identified as sea ice, covering a geographic distance D (Tilling et al., 2018a, 2019). Define a floes size, r, as its “effective radius" — the square root of the floe’s area divided by π (Rothrock and Thorndike, 1984a; Horvat and Tziperman, 2015)~~.~~) We use radius instead of diameter, as appears in some other observational studies, for comparison with model output in Sec. 5. Because the satellite path is at an unknown angle with respect to the (also unknown) floe geometry, any individual floe chord measurement is not a floe size measurement. Converting between suitably processed altimetric floe chord measurements and floe size statistics is therefore the subject of this section. Details on the processing of the CryoSat-2 waveform, used to produce a dataset of floe chords spanning the period 2010-2018, is outlined in Sec. 3 and Tilling et al. (2019).

For a domain of horizontal area A, and over a period of time ΔT that corresponds to several repeat satellite passes, we bin the set of recorded floe chords to form a probability distribution $S(D)$, which we term the “floe chord distribution" (FCD), where $S(D)dD$ is equal to the number fraction of floe chords in A over ΔT with length between D and $D + dD$, and is normalized to one. To collapse all measured chords onto a single independent scalar coordinate (D), we follow the example of turbulence statistics (Batchelor, 1953) and assume that the floe chord distribution data is homogeneous, isotropic, and stationary within the region and time data is collected. In the same region, we define the (non-cumulative) number FSD $P(r)$, where $P(r)dr$

is the fractional number of floes with a size between r and $r + dr$ in A, and is also normalized to one. The FSD inherits the assumptions of homogeneity, isotropy, and stationarity from the FCD. Our objective is to relate the FCD, $S(D)$, or quantities derived from the FCD, to the statistics of the FSD, $P(r)$.

Bayes' theorem relates $S(D)$ and $P(r)$ through conditional probabilities,

$$F(r;D)S(D) = \tilde{F}(D;r)P(r). \tag{1}$$

The conditional probability $F(r;D)$ relates given chord lengths to the floe size distribution that could generate them: ~~$F(r;D)drdD$~~ $F(r;D)dr$ is the probability that floes with size in the range from r to $r + dR$ were sampled given a ~~set of chord lengths in the range from~~ chord of length D~~to $D + dD$~~. The conditional probability $\tilde{F}(D;r)$ relates given floe sizes to the chord length distribution they generate: ~~$\tilde{F}(D;r)drdD$~~ $\tilde{F}(D;r)dD$ is the probability of measuring a floe chord of length from D to $D + dD$ given that ~~floes in the size range~~ a floe of size r ~~to $r + dr$ are being~~ was measured.

This second probability distribution $\tilde{F}(D;r)$ can be derived from first principles under a single assumption: that the chord length distribution that would be sampled from a set of floes of size r is independent of r (equivalently, the floe shape distribution is scale-invariant). Formally, this requirement is,

$$\tilde{F}(D;r)dD = G(\xi)d\xi, \tag{2}$$

where ~~$G(\xi) = G(\frac{D}{r})$~~ $G(\xi) = G(\frac{D}{2r})$ is an unknown function that integrates to 1 over the interval from $\xi = 0$ to 1. Under this assumption, the distribution of possible chord lengths measured from floes of size r has the same functional form independent of r. The probability distribution $F(D;r)$ may be derived by considering the geometric relationship between straight-line satellite passes and the geometry of the floes they pass over. Individual floe shapes are highly variable: making an assumption about the distribution of floe shapes may introduce biases in the statistics derived from the FCD. Yet as we prove in Appendix A, the ability to derive FSD statistics from the FCD does not depend on the precise form of $\tilde{F}(D;r)$ so long as the homogeneous, isotropic, stationary and scale-invariance assumptions are retained, and the evaluation of power-law scaling is in fact independent of $\tilde{F}(D;r)$.

To proceed and arrive at a concrete (although not general) realization of these functions, we will assume all floes are perfect circles. In assessments of the relationship between major and minor axes of individual floes, the "roundness" parameter for a floe is typically within 15% of one ~~(Rothrock and Thorndike, 1984b; Toyota et al., 2011; Perovich and Jones, 2014; Gherardi and Lagomar~~ (Rothrock and Thorndike, 1984a; Toyota et al., 2011; Perovich and Jones, 2014; Gherardi and Lagomarsino, 2015; Alberello et al., 2019) , suggesting that this circular assumption, while simplistic, is broadly appropriate. Nevertheless, it will likely be necessary to amend the analysis below in the future to account for more realistic shape distributions and geometries (e.g., diamonds (Wilchinsky and Feltham, 2006)), regional differences in floe shape properties (such as in regions where shear stress determines sea ice shape (Schulson and Hibler, 1991)), or to evaluate the sensitivity of the results that follow to the assumed shape distribution. Solving for $\tilde{F}(D;r)$ is a geometric problem that relates the possible measured chord lengths to the underlying floe size, and we solve this explicitly for circular floes here. Similar geometric problems have been identified and solved in other fields (e.g., Pons et al., 2006; Nere et al., 2007), and we therefore leave refinement of $\tilde{F}(D;r)$ to future work.

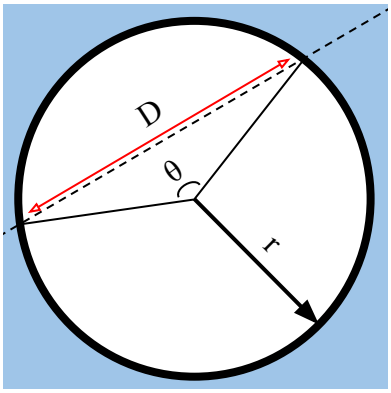

Figure 1. Relating a floe chord to floe size for a circular floe. A satellite track (dashed black line) passes over a floe of radius r (solid black line). The track records a series of echoes of length D, which is the length of a chord (red line) identified by its interior angle, θ.

Consider the special case that all floes are perfect circles, illustrated in Fig. 1. Because there is no correlation between the statistics of local sea ice deformation and pre-determined satellite tracks, an individual recorded floe chord, D, originating from a floe of radius r, was obtained from a satellite trajectory that crosses the floe at a random interior angle θ, thus the distribution of ~~$\theta \in [0, \pi)$ is uniform,~~ θ is uniform. Because of rotational symmetry, we need only consider $\theta \in [0, \pi)$, sampled according to a probability distribution $T(\theta; r) = \pi^{-1}$. The length D is thus a chord of this circular floe, with $D = 2r \sin(\theta/2)$. Accordingly,

$$\tilde{F}(D;r) = T(\theta;r)\frac{\partial \theta}{\partial D} = \begin{cases} \frac{2}{\pi}\frac{1}{\sqrt{(2r)^2 - D^2}} & r > D/2, \\ 0 & \text{otherwise}, \end{cases} \tag{3}$$

which is a probability function that meets the above criterion (2).

The n$^{\text{th}}$ moment of the floe chord distribution $S(D)$, is defined,

$$\langle D^n \rangle \equiv \int_0^\infty D^n S(D) dD = \int_0^\infty dr\, P(r) \int_0^\infty D^n \tilde{F}(D;r) dD. \tag{4}$$

For any function $\tilde{F}(D;r)$ satisfying the scale-invariance above, the right-hand-side may be expressed in terms of moments of $P(r)$ (see Appendix A). For circular floes, using Eq. 3,

$$\langle D^n \rangle = \int_0^\infty dr\, P(r) \int_0^{2r} \frac{2}{\pi} \frac{D^n}{\sqrt{(2r)^2 - D^2}} dD = \int_0^\infty dr\, P(r) \frac{2^{n+1}}{\pi} r^n \int_0^{\frac{\pi}{2}} \sin(x)^n dx = A_n \langle r^n \rangle, \tag{5}$$

where ~~$\frac{D}{r} \equiv \xi = 2\sin(x)$~~ $\frac{D}{2r} \equiv \xi = \sin(x)$, $\langle r^n \rangle$ is the n$^{\text{th}}$ moment of $P(r)$ and the coefficient A_n is,

$$A_n \equiv \int_0^1 \xi^n G(\xi) d\xi = \frac{2^{n+1}}{\pi} \int_0^{\frac{\pi}{2}} \sin(x)^n dx = \frac{2^n}{\pi} \beta B\left(\frac{n+1}{2}, \frac{1}{2}\right).,$$

where B is the beta function. For $n = 0$, 1, 2, or 3, then A_n is 1, $\frac{4}{\pi}$, 2, or $\frac{32}{3\pi}$. Two important FSD-derived quantities are derived from ratios of FSD moments, and therefore can be obtained from the FCD directly: the "representative radius" (Horvat and Tziperman, 2017; Roach et al., 2018a),

$$\overline{r} \equiv \frac{\int_0^\infty r^3 P(r) dr}{\int_0^\infty r^2 P(r) dr} = \frac{\langle r^3 \rangle}{\langle r^2 \rangle} = \frac{3\pi}{16} \frac{\langle D^3 \rangle}{\langle D^2 \rangle}. \tag{6}$$

and the floe perimeter per ice area, a measure of sea ice fragmentation,

$$\mathcal{P} \equiv \frac{\int_0^\infty r P(r) dr}{\int_0^\infty r^2 P(r) dr} = \frac{\pi}{2} \frac{\langle D^1 \rangle}{\langle D^2 \rangle}. \tag{7}$$

These derived quantities are useful because they require no further information about the sea ice (such as its concentration) to compare against modeled FSDs. However, both $\overline{r}$ and $\mathcal{P}$ can represent only those floes whose size is larger than $r_{min} = D_{min}/2$, the smallest possible floe size sampled. For perfect power-law distributions beginning at a scale of r_{min} or before, both metrics are functions of r_{min}. However, for the real FCDs measured here, a maximum floe size exists, and a power-law scaling is not found approaching r_{min}, so the use of such metrics is justified (see Sec. 4). Because of the finite sampling resolution of the altimeter, chords that would originate from floes with a diameter near the sampling resolution may not be observed, and thus $\langle D^n \rangle \leq A_n \langle r^n \rangle$. We explore this uncertainty in Appendix B. For a known floe size distribution, the error decreases exponentially as a function of the distributional moment being considered, though it can be large (20% or more) in pathological cases. For distributional tails characterized by observed scaling exponents (Stern et al., 2018b), and for moments considered here, this uncertainty can be determined systematically and vanishes for measurement spacings smaller than the radius of the most common floe size. This resolution error does not affect the analysis of the ~~the~~ power-law hypothesis, as that analysis is focused on the distributional tail. However, because $\mathcal{P}$ is a proportional to a negative moment of the FCD, it is sensitive to changes in the number of small chord lengths. Because of the measurement uncertainty for smaller chord lengths we will focus instead on $\overline{r}$ which is a positive moment of the FCD.

2.1 Evaluating the Floe Size Power-law Hypothesis with Floe Chord Data

Suppose the FSD $P(r)$ has a power-law tail that begins at some specified value r_1. Then for $r > r_1$, $P(r) \equiv P(r; \alpha, C) = Cr^{-\alpha}$, for an unknown coefficient C and power-law slope α. Integrating Eq. 1 over all r,

$$S(D) = \int_0^\infty \tilde{F}(D; r) P(r) dr, \tag{8}$$

where ~~we leverage that because it is a probability distribution,~~ the integral of the left-hand side of Eq. 1 is equal to $S(D)$ as $\int F(r;D)dr = 1$. Under the assumption of Eq. 2, if P is a power law, so is $S(D)$ (Appendix A). For circular floes,

$$S(D) = \frac{2C}{\pi} \int_{r_1}^{\infty} \frac{r^{-\alpha}}{\sqrt{(2r)^2 - D^2}} dr. \tag{9}$$

Because of the sampling resolution of the altimeter there is a minimum resolved chord scale D_{min}. If $D_{min} \ll D^* \equiv 2 \cdot r_1$, there is an explicit solution for $S(D)$, a power-law distribution over the range (D^*, ∞)

$$S(D) = C \cdot B\left(\frac{1}{2}, \frac{\alpha}{2}\right) \frac{2^{\alpha-1}}{\pi} D^{-\alpha} \equiv C_\alpha D^{-\alpha}. \tag{10}$$

where B is the beta function. The coefficient C_α is a multiplicative factor independent of size, and the power-law exponent for a FCD is the same as the exponent for FSD, where the two are related by Eq. 1.

Moments of a power-law tail can be evaluated explicitly (for $\alpha > n+1$),

$$\langle r^n \rangle = C \int_{r_1}^{\infty} r^{n-\alpha} dr = C \frac{r_1^{n+1-\alpha}}{n+1-\alpha}. \tag{11}$$

Then for both the FCD and FSD, the ratio of ~~any~~ two moments is independent of the unknown coefficient C, i.e.,

$$R_{n,\epsilon} \equiv \frac{\langle D^n \rangle}{\langle D^{n-\epsilon} \rangle} \approx \frac{\langle D^{n+\epsilon-1} \rangle}{\langle D^{n-1} \rangle} = D_{min}^{\epsilon} \frac{n-\alpha}{n+1-\epsilon-\alpha} \frac{n-\alpha}{n+\epsilon-\alpha}, \tag{12}$$

valid for ~~$n+1<\alpha$~~ $n+\epsilon<\alpha$. The power-law coefficient can be obtained for any n, ϵ as,

$$\alpha_{n,\epsilon} = n + \epsilon \frac{R_n}{R_n - D_{min}^{\epsilon}} \frac{R_{n,\epsilon}}{R_{n,\epsilon} - D_{min}^{\epsilon}} = \text{constant}. \tag{13}$$

In the analysis below we will arbitrarily select only $n = 0.5, \epsilon = 1$ for comparison (for scaling coefficients $\alpha > 1.5$, the bulk of reported power-law coefficients are in this range: Stern et al., 2018b). Because the observations will not be perfect power-law distributions, we will use $\alpha_{0.5,1} \equiv \alpha^*$ as an estimator. A second estimate of the power-law scaling coefficient, $\hat{\alpha}$, is computed via the maximum likelihood estimator (Muniruzzaman, 1957; Clauset et al., 2009; Virkar and Clauset, 2014) (details in Appendix C) as,

$$\hat{\alpha} = 1 + \frac{N}{\sum_{i=1}^{N} \ln \frac{D_i}{D_{min}}}. \tag{14}$$

where N is the number of chords. If the ~~condition that $n+1<\alpha$ is met~~power law hypothesis holds, then the ~~agreement of these~~ two estimates of α ~~is a necessary, though not sufficient condition for~~ agree, although the aggrement of $\hat{\alpha}$ and $\alpha_{n,\epsilon}$ is not sufficient to confirm the power-law hypothesis~~to hold for a well-sampled distribution. We provide code and a comparison tool in~~. In the Supporting Information (Text S1 and File S1)~~to examine the accuracy of these estimates, showing they are accurate and in agreement~~, we include Matlab code that compares the two estimates, and shows that they agree even for small ($N < 25$)

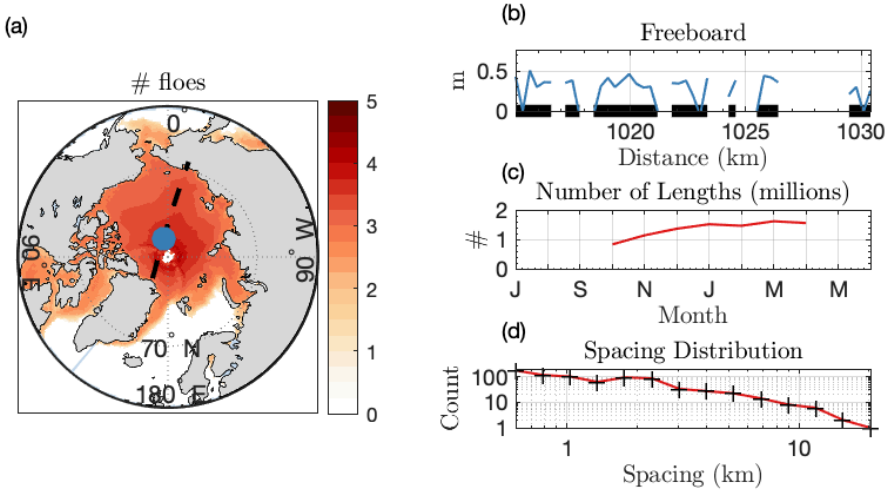

Figure 2. Constructing a FCD from altimetry. (a) Base 10 logarithm of the number of floe chords identified, binned into the CESM grid, across all CryoSat returns in the Arctic from 2010-2018. Black line is a single satellite track on January 21, 2014. (b) Subsection of the track centered on the blue dot in (a). Blue line is freeboard of sea ice in radar echoes defined as "floes" along the track. Black lines are chords identified from the freeboard retrieval. (c) Total number of chords measured in each month in the Arctic. Plot is centered on January 1. (d) FCD for the satellite track depicted in (a). Black marks on x-axis are the logarithmically spaced chord length bins.

sets of power-law distributed data. ~~We caution again that the easier-to-apply~~ While in practice Eq 13 is ~~applicable only~~ easy to apply, it only holds when $\alpha_{n,\epsilon} > n+1$~~. The~~ , and unlike the method of Clauset et al. (2009)~~is preferred because it permits goodness-of-fit tests for the power law distribution, estimates of the beginning of the range or applicability of the power law, D_{min}, and a method for evaluating the statistical likelihood of a power law decay for any n, which we exploit in Section 4~~, it does not allow for a robust statistical analysis of the power-law fit, and should only be used when the data is assumed to follow a power-law already.

3 Climatology and Trends in Floe Properties Derived from CryoSat-2 Altimetry

We apply the analytic technique described in Sec. 2 to a floe chord data set constructed from the CryoSat-2 radar altimeter processed by the Center for Polar Observation and Modelling (CPOM) over the period from October 2010-present (CPOM data products are available at http://www.cpom.ucl.ac.uk/csopr/seaice.html). CryoSat-2 radar echo returns are defined as "lead", "floe", "open ocean" or "ambiguous" ~~at an approximately constant along-track spacing D_{min} =300 m~~ according to waveform shape and sea ice concentration (Tilling et al., 2016, 2018b), at an approximately constant along-track spacing D_{min} =300 m. Floe chords are defined as a continuous sequence of ~~two or more "floe " echos~~one or more "floe echoes", with a gap of ~~at most one echo permitted in sequence, and single isolated floe returns eliminated, to account~~ one ambiguous echo permitted within a floe sequence to allow for anomalous returns. A chord length is taken from the midpoint of the first to the midpoint

of the last radar echo. Individual chord lengths ~~may be underestimated in cases where~~ can be underestimated when continuous floes are separated artificially by producing two or more ambiguous echoes in sequence~~. A chord length is taken from the midpoint of the first to the midpoint of the last radar echo.Floe chord lengths are not measurements of floe size, and do not resolve regions of small floes, as the~~ , or when highly reflective leads dominate the waveform return close to the floe edge and cause measurement dropout (Tilling et al., 2019). Lead contamination, or "snagging" (Armitage and Davidson, 2014) is more likely when the altimeter cuts of a small section of a floe, i.e. for small values of θ. Overestimates of chord length can also occur when ice floes are in close contact with neighboring floes. Therefore, floe chord lengths should be considered a satellite-derived product, not a true measurement of floe size. The minimum chord length retrieval D_{min} is limited to the CryoSat-2 footprint (~~~~ 300 meters along-track) (see the discussion in Appendix ~~B~~B). However, surface discrimination via altimetry is highly accurate in months without melt ponds, (Peacock and Laxon, 2004; Guerreiro et al., 2017; Quartly et al., 2019), giving confidence that ~~two consecutive floe echos , the minimum length scale represented here,~~ floe echos represent a coherent length of ice. More details on the details of chord identification may be found in Tilling et al. (2019). Indeed, this raw floe chord data has been used successfully to reduce biases in altimeter-observed satellite sea ice thickness estimates from ~~satellite~~ altimeters with different footprint sizes ~~(Tilling et al. , 2018a, 2019).~~ Tilling et al. (2019). Here we analyze the sea ice floe size distribution using that floe chord product.

Figure 2 shows an example of floe chord data for a single CryoSat-2 track over the Arctic on January ~~14, 2018.~~ 21, 2014. Freeboard values for echoes discriminated as "floe" are plotted in Fig. 2b as a function of the along-track distance in km, and correspond to the ~~red~~ blue circle in Fig. 2a. Floe chords are identified as black segments in Fig. 2b. The histogram of all 741 identified chords for this single satellite pass is shown in log-log space in Fig. 2d.

The full CryoSat-2 dataset examined here spans the time period from October 2010 to November 2018, and floe chords measured using the above technique are binned into the CICE sea ice model's two-dimensional sea ice grid for each month and year to facilitate comparison with model products. This implies that the principles of isotropy, homogeneity and stationarity of the FCD, required to produce such a distribution, are invoked on the length scale of the CICE model grid and time scale of a month. For every grid cell i, month m, and year y, we have a vector of floe chords $\{D_{i,m,y}\}$ from which we build a FCD. The base 10 logarithm of the total number of floe chords recorded in each grid cell per month is shown in Fig. 2a. Because the satellite passes are densest near the pole, the measurement density is highest near the pole as well. Fig. 2c shows the number of Arctic measurements in each month. Sea ice type from CryoSat-2 is not available during summer months, as melt ponds make it difficult to discriminate between leads and ponded floe surfaces, and we do not include measurements from May to September. Across the entire set of satellite tracks included here, 11 million chord lengths are recorded in the Arctic.

Figure 3a shows the seasonal cycle of Arctic representative radius over the CryoSat-2 period obtained by applying Eq. 6 to the binned CryoSat-2 floe chord product. Individual years are plotted as thin lines, and the climatological average is shown in red. Details on how temporal and spatial average statistics are computed is included in Appendix D. During the months of October-December, the climatological representative radius is roughly 35% larger (7.06 km vs 5.18 km) than February-April. This seasonal cycle is broadly consistent across years. We interpret this seasonal cycle in size over time as due to the formation of large first-year ice pans in October which are later fractured into smaller floes throughout the winter months.

Fig. 3b shows annual-average representative radius in red for each full year from 2011-2017, with thin lines corresponding to the individual months within that year. Seasonal variability is significantly larger than inter-annual variability. There is no statistically significant linear trend at the p=0.05 level.

The geographic variability of representative radius over the “early winter" (October-December) and “late winter" (February-April) periods are shown in Fig. 3c-d, for all grid areas. We display only those areas with at least 25 recorded floe lengths in each month ~~within~~ during the averaging period. ~~The 25 measurement threshold was chosen as the mean statistics presented here were insensitive to smaller or larger thresholds where a majority of chords are included (see~~ In Supporting Information Text S2 and Fig S1~~)~~, we examine the sensitivity of bulk FSD statistics to this threshold, finding similar seasonal cycles and climatologies. The largest representative radii in the Arctic lie ~~along the Canadian archipelago~~in the interior Arctic near the pole, with a tongue of large floes that extends along the ~~American~~ Canadian Arctic in late winter. There is a notable increase of representative radius with latitude. In the Supporting Info Fig. S2, we show that this relationship cannot be explained as a result of the increasing density of measurements near the pole and may therefore be a geophysical signal. The smallest representative radii (below 1 km) lie in Bering Strait and the Russian Arctic in early winter, and in the Laptev Sea in late winter. The difference in representative radius ~~from~~ between fall and spring is accounted for by the reduction of floe sizes in regions near the Arctic interior (see Fig. 6).

4 Evaluating the Power-law Hypothesis Using Floe Size Statistics Derived from CryoSat-2

Given a collection of chord lengths, we would like to examine whether it is distributed according to a power law. Under the assumptions of Sec. 2, the scaling behavior of the FSD is the same as of the FCD (see Appendix A). We use the statistical methodology outlined in (Clauset et al., 2007, 2009; Virkar and Clauset, 2014) (which we term the MLE method) to evaluate shape parameters of the most likely power law fit and to test its plausibility. This method has been used to evaluate power-law behavior in recent FSD model Horvat and Tziperman (2017) and observational studies Hwang et al. (2017); Stern et al. (2018b) and proceeds as follows:

1. **Lower-truncate the FCD**. First identify a minimum chord scale, D^*, above which we hypothesize a power law tail, and analyze only those floe chord measurements. We either (a) choose D^* ~~as the peak of the FCD (generally equal to D_{min}~~to be 900 m (to reduce the impact of small-size sampling errors discussed in Sec. 2) or (b) use the scheme described in Clauset et al. (2007) to evaluate the most likely value of D^* for a power law tail. The length of this lower-truncated distribution is N. In the descriptions that follow, we use the subscript all to describe case (a) and $tail$ to describe case (b).

2. **Compute power-law scaling estimates and parameter uncertainty**. We obtain two estimates of the FCD scaling estimate: either computing α^* via Eq. 13, or computing $\hat{\alpha}$, and uncertainty estimates in both $\hat{\alpha}$ and D^* via the MLE method (Eq. 14). That the two estimates of α agree is a necessary condition for the FCD (and thus FSD) to be power-law distributed.

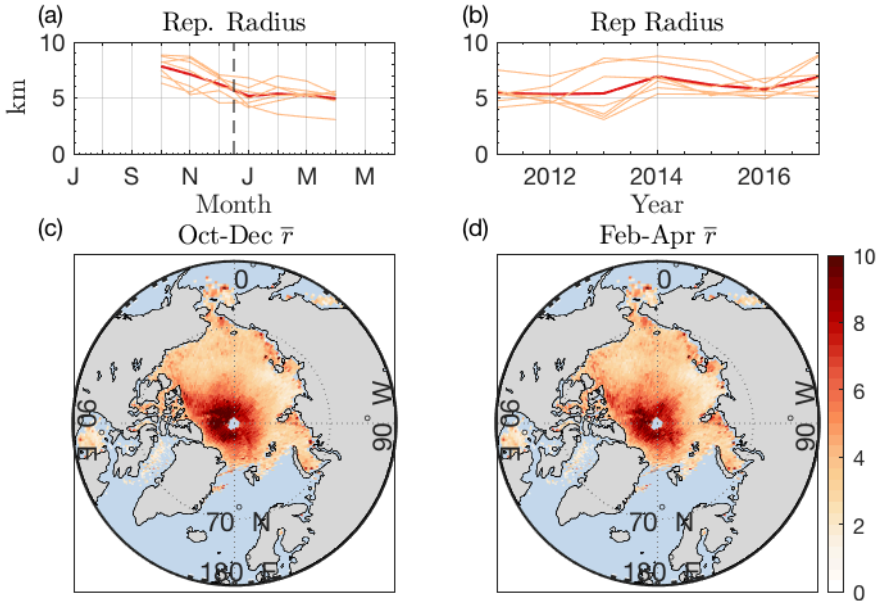

Figure 3. Top row: Temporal and geographic variability of Arctic representative radius. (a) Climatology of Arctic-average representative radius in units of km (red line). Thin lines are individual CryoSat-2 years. (b) Annual-average Arctic representative radius (red line). Thin lines are average in individual months. (c) Climatological representative radius in months October-December. (d) Same as (c) but for February-April.

3. **Examine the plausibility of the power law fit**. We generate M FCDs of size N (the same number of synthetic chords as observed chords), with each synthetic FCD drawn from the hypothesized power law distribution $P(\hat{\alpha}, D^*)$. For each of these synthetic FCDs, we compute the Kolmogorov-Smirnov distance between it and the hypothesized power law model that generated it, $P(\hat{\alpha}, D^*)$. We also compute the distance between the observed FCD and $P(\hat{\alpha}, D^*)$. A p-value, p, is equal to the fraction of those M synthetic FCDs that are "further away" from the hypothesized power law model than is the observed FCD. We use $M = 10,000$, which permits computation of p within 0.005 (Clauset et al., 2009), and rule out the ~~power law fit using the conservative~~ power-law hypothesis under the condition $p < 0.1$ ~~of Virkar and Clauset (2014)~~ (Virkar and Clauset, 2014).

We note that a "power law" describes the scaling of a distribution's tail. Previous observational studies have discussed "double power laws" (i.e., Toyota et al., 2011), i.e. ~~we can rule out the power law hypothesis when a random sampling from the hypothesized~~ two power-law ~~distribution is closer to that power-law distribution than the observations more than 90% of the time.~~ distributions of different exponent joined at a specified scale. The methods employed here would capably capture the large-size power law scaling but not the small-scale scaling. Such "double power laws" are necessarily scale-variant, and

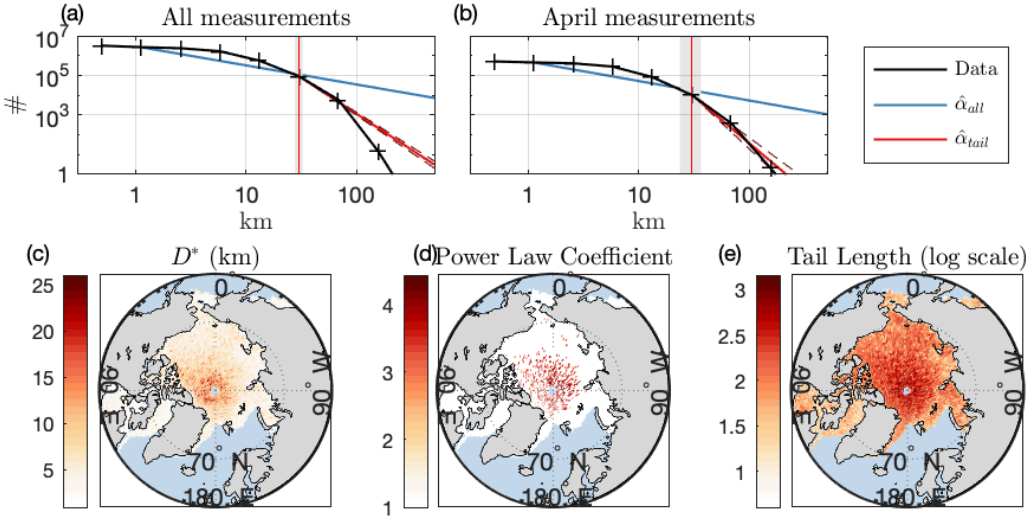

Figure 4. Examining the power-law hypothesis. (a) Histogram of all chord lengths recorded in the Arctic for the months November-April (black). Bin ~~edges are shown as~~ centers indicated by hashes ~~on the x-axis~~ and are logarithmically spaced. Blue line is power-law fit to all observed sizes according to eq. ~~11, with shading the difference between blue line and black line~~14. Red line is power-law fit to the tail~~, with~~ . Dashed red ~~shading~~ lines are fit lines using the ~~difference between red line and black line~~± 1 standard deviation values of $\hat{\alpha}$. Red vertical line is the most likely beginning of the power law tail, D^*, with shaded region ± 1 standard deviation in D^*. (b) Same as (a), but for measurements in April. (c) Maximum likelihood estimate of the beginning of the power law tail, D^* (in km) for all measurements at each geographic location over the observational period. Only locations with $N > 1000$ are plotted. (d) Maximum likelihood estimate of power law tail exponent, $\hat{\alpha}_{tail}$, for the same points. Colored values have more than 200 chord lengths in the tail and $p > 0.1$. Zero values are those locations plotted in (c) but where either $p < 0.1$ or there are less than 200 measurements in the tail. (e) Number of chord lengths in the tail (above D^*) at each location.

require at least 3 parameters to describe. The conceptual and mathematical simplicity of the "power law hypothesis" does not apply in such a case, and we do not consider them here.

The MLE method is a rigorous test of the power-law hypothesis that eliminates potential human bias when interpreting observational data. To illustrate why this is important, we first consider the entire set of 11 million chord lengths recorded in the Arctic in all months (October-April), spanning ~~3 orders of magnitude~~ a length range from 300 m to 100 km. The histogram of these floe chords is the black line in Fig. 4a (hashes on ~~the x-axis show the~~ black line are the logarithmically spaced bin centers). ~~With the most commonly recorded floe size $D^* = D_{min} = 300$m, $\hat{\alpha}_{all} = 1.56$~~ Beginning from $D^* = D_{min} = 900$m, $\hat{\alpha}_{all} = 1.97$ (blue line) and ~~$\alpha^*_{all} = 1.70$~~ $\alpha^*_{all} = 2.05$ (not shown). The observations are further away from synthetic data drawn from $P(\hat{\alpha}_{all}, D^*)$ in each of the $M = 1{,}000$ random draws ($p_{all} = 0/1000$) and we reject the power law hypothesis for these measurements. We note that if the resolution bias explored in Appendix B proves to be larger than expected, the under-representation of small floe lengths may affect the analysis of the full distribution.

Examining the tail of the distribution in Fig. 4a, the maximum likelihood estimate of D^* is ≈ 15.0 km (red vertical line, vertical shaded region is the range of uncertainty for D^*), above which there are ~40,000 chord length measurements between 24.7 km and 99 km (0.4% of the dataset). On the truncated FCD, ~~$\hat{\alpha}_{tail} = 4.56$~~ $\hat{\alpha}_{tail} = 4.65$ (red line, dashed lines are uncertainty ranges for $\hat{\alpha}_{tail}$), and ~~$\alpha^*_{tail} = 4.66$~~ $\alpha^*_{tail} = 4.67$ (not shown), similar to the large-scale roll-off reported in observations Toyota et al. (2016). Even when restricted to the FCD tail, $p_{tail} = 0/1000$.

Finding no statistical basis for a power-law fit to the tail in Fig. 4a underscores the challenge in using the human eye to observe power law scaling. While the black and red lines in Fig. 4a ~~*appear*~~ appear similar across much of the range of sizes above 24.7 km, ~~by~~ examining the misfit between the power law estimates and the data ~~(shaded values in Fig. 4a, blue is for the entire distribution and red is for the tail), the~~ show that the two curves in fact differ significantly across the entire fit range. A misfit error can be defined as,

$$E = \left\langle \frac{|P(x_i, \hat{\alpha}_{tail}, D^*) - P(x_i)|}{P(x_i, \hat{\alpha}_{tail}, D^*)} \right\rangle \tag{15}$$

where the x_i are the bin locations, angle brackets denote an average over the relevant bins, and $P(x_i)$ are the observed histogram values. Over the range from 24.7 km to 100 km, the misfit error is 33%. The visual agreement, misfit error, and apparent slope and shape of the distribution depend sensitively on the bin spacing and the logarithmic plotting.

~~Assuming a multiscale power law of floe sizes when the power law hypothesis is invalid~~ Sea ice parameterizations that assume a power law distribution may significantly bias sea ice ~~parameterizations. Imposing a distributional shapein the presence of scale-selective FSD evolution~~ statistics. The imposition of any fixed distributional shape, when FSD dynamics are scale-variant, leads to implicit non-local redistribution of sea ice ~~among~~ between floe size categories (Horvat and Tziperman, 2017). ~~For example, we may compare the~~ To see this in practice we compare the difference in Arctic-wide representative radius, $\overline{r}$, which is used in parameterizations of ~~wave-ice interaction and sea~~ wave attenuation and ice thermodynamics, between the ~~full Arctic FCD and its most likely~~ most-likely power-law ~~distribution. The representative radius (of floes larger than D_{min}) is 10.2 km when applying~~ fit to the data and the "true" value obtained via Eq. 6~~to the observed FCD (black), but~~ . The observations yield $\overline{r}$ =10.2 km, versus 34.5 km ~~applied to the fitting line (blue). In the tail (i.e., for~~ for the power-law fit. Examining only the tail of the distribution (chord lengths above 24.7 km) ~~, the representative radius is similar: 24.4~~ yields better agreement: 23.7 km for the ~~fitting line and 23.7 km for the observations. Yet less than~~ observations and 24.4 for the fit line. Yet this tail constitutes just 1% of ~~chord lengths are larger than 24.7 km, accounting for~~ all measured chord lengths, corresponding to just 18% of ~~the~~ total ice area ~~, and just~~ and 4.5% of the perimeter per square meter (Eq. 7).

Segmenting the chord length data into individual months in the Arctic, there are none where $p_{all} > 0$. Examining only the tail of each month's distribution, $p_{tail} < 0.1$ in all months. Only in April is there a non-zero ~~$p_{tail} = 0.05$~~ $p_{tail} = 0.04$, for which the analysis of Fig. 4a is repeated as Fig. 4b. In April, ~~$\hat{\alpha}_{all} = 1.62$~~, $\hat{\alpha}_{all} = 1.99$, $\hat{\alpha}_{tail} = 5.70$, and $D^* = 30.7$ km. The tail consists of 1618 measured chord lengths up to 97.5 km, accounting for 8% of the total floe area and 1.4% of the perimeter per square meter. The misfit error between the April FCD tail and $P(\hat{\alpha}_{tail}, D^*)$ is 76%. Accumulating all measured chord lengths from October-May into the CESM model grid, we find zero locations that support a power law distribution across the range

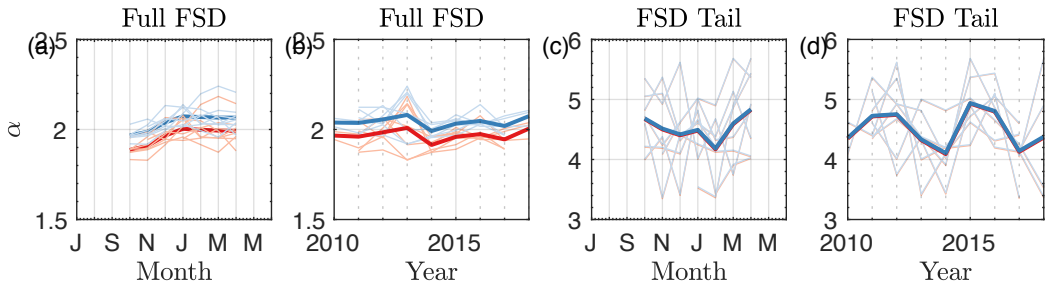

Figure 5. Top row: Temporal variability of power law fits to Arctic FCDs. (a) Estimate of the most likely power-law scaling coefficient for all recorded floe chords as a function of month over all years, calculated from the MLE method Eq. 14 (red lines) or Eq. 13 (blue lines). Thick lines are climatological averages, thin lines are individual years. Plot is centered on January 1. (b) Like (a), but plotted for individual years over all months. Thick lines are average over months plotted in (b) and thin lines individual months in each year. (c-d) same as (a-b), but for the distributional tail starting from D^* computed using the MLE method. "Arctic" refers to points above 60°N

of measurements (i.e., $p_{all} > 0.1$). For grid areas with $N > 1000$, we show the value of D^* computed using the local FCD in Fig. 4c. Values of D^* range from 2 kilometers along the Russian Arctic to more than 10 km near the Pole.

While most of the Arctic has at least 1000 total measurements across all years, FCD tails ($D > D^*$) are not as well-sampled. We investigate these tails including regions with at least 200 measured floe chords larger than D^*. The percentage of geographic areas with at least 1000 total measurements that have a tail with at least 200 measurements is 44%; on average D^* is 5.4 km for these regions. For most of these regions we can not rule out a power-law tail. For the subset of regions with 1000 total measurements, 200 measurements in the tail, and where the power law hypothesis cannot be ruled out, the average D^* is 6.5 km and average $\hat{\alpha}_{tail}$ is 3.34, within the typical range of Arctic FSD measurements (Stern et al., 2018b). In fig. 4d we show the values of $\hat{\alpha}_{tail}$ at these locations, with colored cells those where $p > 0.1$ and the tail has at least 200 measurements. In Fig. 4e we show the base 10 logarithm of the MLE tail for all geographic locations. Those regions for which a power law cannot be ruled out are generally those with the largest floes and the highest sampling, clustered near the central Arctic. The weakest support for a power-law tail is in the Chukchi and Beaufort seas, where power-law floe size distributions have often been reported. We note that our choice of tail length plays an important role in whether the power-law hypothesis is rejected in the tail across the Arctic. For example, the fraction of Arctic regions with at least 1000 total measurements, a tail of at least 100, 200, and 400 measurements, and that does not reject the power-law hypothesis is 72%, 52%, and 15%, respectively. The better-sampled the FCD/FSD, the more likely the power-law hypothesis is rejected.

Scaling coefficients can provide useful information about the distributional shape. In Fig. 5(a-d) we show the seasonal and inter-annual variability of power-law estimates in the Arctic. Figure 5a plots the climatology of the power law scaling estimates when including all measured chord lengths in dark red (using Eq. 13) or blue (using 14). Individual years are thin red or blue lines. The two estimates ~~consistently disagree , which as discussed previously is~~ disagree — as their agreement is necessary for the power law hypothesis to be true (see Sec. 4, SI Text S1), this alone is sufficient to rule ~~out the power-law hypothesis~~it out. There is ~~no trend or~~ a seasonal cycle in the power-law fitting ~~for~~ to the full distribution, with α_{all} increasing (steepening) from

September to January and remaining flat until April, and no significant linear trend at the p=0.05 level for the annual-average value of α_{all}. Fig. 5(c-d) repeats this analysis on the tail of those monthly distributions. In this case, the two estimates agree well. There is a different seasonal cycle in the steepness of the distributional tail: shallowest in early winter and steeper in late winter~~, inverse to the trend in representative radius exhibited in Fig. 3a.~~. This indicates that the changes across the winter months may be due to a reduction of the largest floes and a steepening of the distributional tail~~.~~, although there is significant inter-annual variability among these estimates. A similar seasonal cycle to that found in Fig. 6(a,c), with an FSD that steepens from September to April, was found in image analysis of floes in the Beaufort and Chukchi Seas (Stern et al., 2018b), with $\alpha \approx 2.5$, although the distribution steepened monotonically over that period. There is no significant linear trend at the p=0.05 level in the annual-averaged FSD tail slope (Fig. 5d).

5 An Example Model-observation Comparison of Floe Size Variability

With the gridded data provided above, we may now directly compare development-stage sea ice models that incorporate FSD effects to observations. To do so, we use the Roach et al. (2018a) prognostic model for the FSD/FSTD, based on the Horvat and Tziperman (2015) theoretical FSTD framework, implemented into CICE 5.1.2 (Hunke et al., 2015) sea ice model. The FSTD is a sea ice state variable, subject to interaction of five key physical processes: lateral growth, lateral melt, fracture by ocean surface waves, welding of floes in freezing conditions and wave-dependent new ice growth (Horvat and Tziperman, 2015, 2017; Roach et al., 2018a, b). Previously published model runs (Roach et al., 2018a) ~~investigated~~ focused on the impact of the FSD on lateral melt, ~~particularly important for floe sizes below 300 m (Steele, 1992), necessitating a maximum floe size of~~ which is largely driven by small floes (Steele, 1992), and so floe sizes above 1 km were not considered. As a larger range of scales is ~~resolve~~ resolved in the CryoSat-2 observational product, we conducted a model run that extended the floe size categories to scales larger than 1 km, using 24 logarithmically-spaced floe size categories from 0.5 m to 33 km.

This FSTD model simulation is coupled to a slab ocean model and the WAVEWATCH III ocean surface wave model (Tolman, 2009), forced by the JRA55 atmospheric reanalysis ~~(Kobayashi et al., 2015) from the pre-industrial period to 2016.~~ (JRA-55, 2013) over the period from 2000-2016. These wave-coupled runs are branched at year 2000 from a standalone sea ice run from 1975-2000, spun-up using repeated 1975 atmospheric forcing.

Additional model physics beyond those processes outlined in Roach et al. (2018a), have been added to determine the initial size of newly formed sea ice floes as a function of the ocean surface wave field. Details on this new parameterization, model initialization, and spin-up, are described in Roach et al. (2019). Recalling the finite measurement resolution of the CryoSat-2 dataset, the modeled representative radius is calculated ~~including only~~ only including floe size categories from 300 m and larger.

Fig. 6(a-b,d-e) compares modeled and observed climatologies of Arctic representative radius (for floes larger than 300 m) averaged over 2011-2016 and the months of October-December (a,b) and February-May (c,d). Geographic variability of representative radius is broadly similar between model and observation: the largest floes lie in the Arctic interior~~and Canadian Archipelago~~, with regions of smaller floes in the ~~Straits~~ straits and continental margins. Across the interior Arctic, simulated

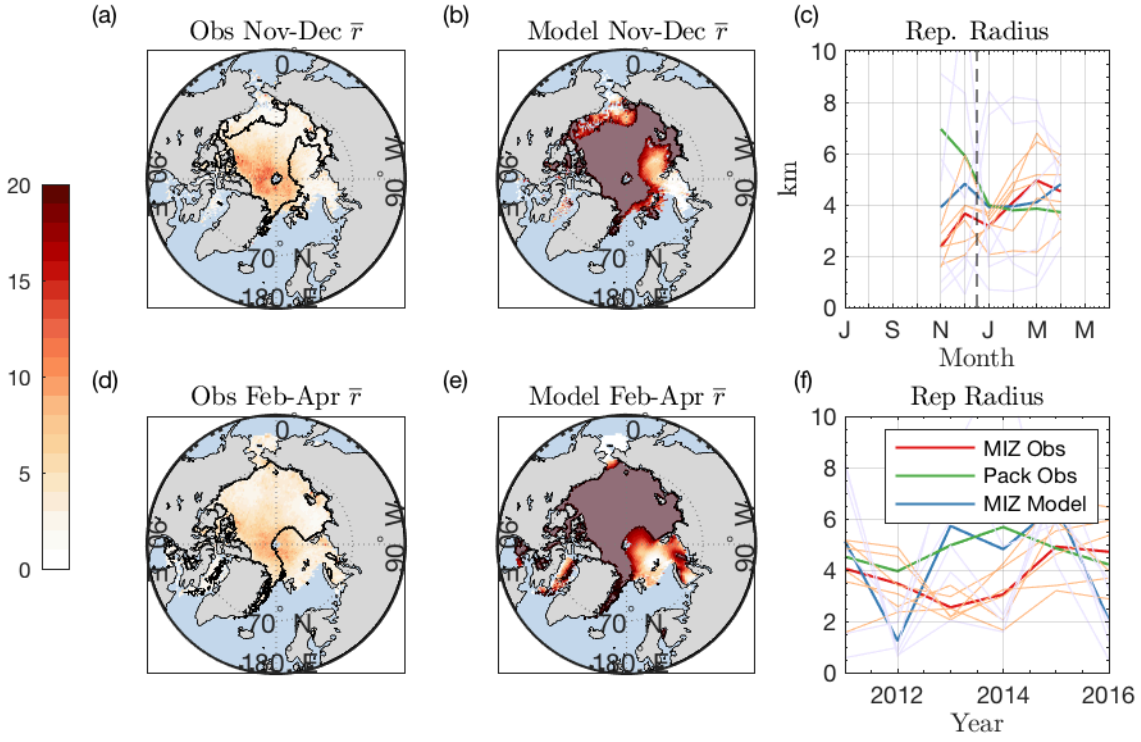

Figure 6. Geographic and climatological comparison of modeled and observed representative radii. (a-b) Average representative radius from November-December in (a) the CryoSat-2 observational dataset and (b) the FSTD model. Grey shaded regions in (b) are the interior of contours in (a), which represent “pack ice" unaffected by waves in the model simulations. (c) Climatology of Arctic-average representative radius in units of km for the MIZ in observations (red) and modeled (blue). Green line is the annual average for the “pack", the excluded regions in (b). Thin lines are averages in individual years from 2011-2016 in the MIZ. (d-e) same as (a-b), but for the months of February-April. (f) Annual-average Arctic representative radius for wave-affected regions in MIZ observations (red), MIZ model (blue), and pack ice observations. Thin lines are average in individual months in the MIZ observations.

representative radii are significantly larger than are found in the observations, as the Roach et al. (2018a) FSTD model does not include processes that break up large floes in the absence of ocean surface waves. To compare seasonality between model and observations, we compare only those regions that experience wave fracture in the model runs, areas we collectively term the marginal ice zone (MIZ). The MIZ is defined by excluding categories that do not experience wave fracture in a given month (see Appendix D), shown as the contoured regions in Fig. 6(a-b,d-f) and greyed out in Fig. 6(b,e)). All excluded “pack ice" regions have modeled representative radii greater than 18 km. The MIZ region accounts for 37% of grid areas with at least 25 chord measurements in months from October-December and 35% of such areas for the period February-March. Note that the month of October is absent from these plots, because no well-sampled regions are classified as MIZ across all model years according to the criteria outlined in Appendix D.

Fig. 6(c) compares the observed (red) and modeled (blue) Arctic-average representative radii for the MIZ across over the period 2011-2016 as in Fig. 3(a). The seasonal cycle of representative radius in the MIZ is different in the observations (red line, thin orange lines are individual months) than when all geographic regions are included (Fig. 3a). The seasonal cycle of representative radius in the “pack ice" region (i.e. not the MIZ) is shown as a green line in Fig. 6c. In the MIZ, average representative radii are smaller (on average 4.17 km vs vs. 6.49 km in the pack ice region). In contrast to the seasonal variation across all geographic regions (Fig. 3a) as well as in the pack ice, floes are larger in February-April than in November-December (5.40 km vs 3.15 km). In both the MIZ and pack ice regions, however, average representative radius is similar in late winter. The largest difference between the two regions is from November-December, where representative radii are more than twice as large in the pack ice than the MIZ.

Fig. 6(f) shows the annual average representative radius in the MIZ (red), pack ice (green) and modeled MIZ regions (blue). Modeled MIZ representative radii have a similar magnitude compared to the MIZ observations, though these regions have smaller floes than the interior. To address the scale mismatch between the too-high modeled floe sizes and observed representative radii in the interior Arctic, as well as the strong and different seasonal cycle in representative radius in both regions, modeling efforts must include additional mechanisms for reducing floe size in the Arctic interior away from waves, such as mechanical fragmentation (Toyota et al., 2006; Rynders et al., 2016) or ridge dynamics (Roberts et al., 2019), to obtain realistic representative radii across the entire Arctic, as these processes are not present in the model used to make this comparison.

6 Conclusions

Here we developed and demonstrated a method for deriving the statistics of the sea ice FSD from satellite radar altimeter measurements of chord length. This method provides the first ~~global, high-resolution~~ pan-Arctic accounting of climate-relevant quantities derived from the FSD, permits testing of existing scaling laws previously used to characterize distributions of floe size, and allows for gridded comparisons between FSD models and observations. Using this new technique we produced climatological, annual-average, and geographic mean moments of the Arctic FSD across ~~3 orders of magnitude of floe size.~~ a range of resolved length scales from 300 m to 100 km.

With the combination of satellite altimetry and mathematical theory, we were able to rigorously examine the “power-law hypothesis" related to the FSD under simple assumptions about the underlying floe chord data and the fidelity of CryoSat-2 satellite retrievals. Segmenting measurements by geographic location, by month, and by year, we find limited statistical basis for a power-law scaling beginning below about 6.5 kilometers. In a limited number of geographic locations, we find the observational data cannot rule out power-law scaling, but for typical sizes above about 6.5 kilometers. Assuming a power-law floe size distribution can bias sea ice model output and conceptual understanding. The geographic variability and lack of consistent multi-scale behavior reinforces the need for sea ice models to account for floe-scale processes rather than diagnose a distributional shape.

Observations that span the polar regions and different years and seasons are valuable for future refinement of process-based models of the FSD. In Sec. 5, we demonstrated how such model-observation comparisons can be made and can provide useful insights for model developers. At present, some general features of floe size evolution (in particular the magnitude and seasonal cycle of the representative radius) are broadly similar between model and observation in the marginal ice zone. Yet there is a significant scale mismatch in the interior Arctic between ~~a simulation~~ the presented simulations and this observational product, because of missing fragmentation physics in the absence of ocean surface waves. Floe size modeling efforts have focused on ~~the~~ marginal ice zone processes (Horvat and Tziperman, 2015; Zhang et al., 2015), and particularly floe sizes below about 1 km because these small floes play an important role in sea ice thermodynamics for floe sizes. The CryoSat-2 observations, however, are best suited to resolving floe chords of ~~300 m~~ several hundred meters and above. New satellite altimeters like ICESat-2 have the potential to increase the chord length resolution to scales of 20-100 m and provide insight at smaller scales.

We emphasize strongly that refinement may be necessary to apply this method for operational purposes, trend analysis, and further model validation. ~~We have~~ This paper has focused on the framework for making altimetric measurements of the FSD and comparison to model output, but the obtained chord lengths and distributions have not been carefully validated against other observational methods, and this will be necessary before further application of this method. Before doing so, we have tried to outline the most significant uncertainties in the ~~application of this~~ method. The typical assumptions of homogeneity, isotropy, and stationarity are invoked here at the length scale of the CICE model grid and time scale of one month. These statistical assumptions may not be satisfied if, for example, the number of measurements in a given region in one month is insufficient to sample the known anisotropy of the sea ice floe field, and additional passes change the mean chord length significantly (see Supporting Information Text S2 and Fig S1). The assumption of scale-invariant sampling, ~~and structural uncertainty that arises because of~~ observational uncertainty because of the finite sampling resolution, analysis of ambiguous returns, and the accuracy of retrievals in regions of thin sea ice may also affect the inferred size of sea ice floes. This in turn may affect the climatologies described in this study.

While processed CryoSat-2 ~~product~~ data has been validated against both visual imagery and ground-based observations, it was not designed with this application in mind — additional quality control may be necessary for climate studies of changing floe properties. The ~~assumption that chord length measurements are accurate at the scale of the satellite footprint, which affects the assessment of a multi-scale power law, will need to be examined by comparing these results to other altimeters. The positive findings of~~ positive comparison between model and observation in Section 5 could also be due to a compensation between

these measurement uncertainties ~~.~~and will need to be re-examined in future validation work. Yet observational uncertainties regarding, for example, the floe shape distribution can be roughly estimated at the order of the error in "effective radius" obtained for circular floes ($r = \sqrt{A/\pi}$) or a square ($r = \sqrt{A/4}$), a relative error of 25%. To constrain model results beyond this scale of error will require further refinement. However, as shown in Fig. 6, at present the model-data mismatch in the interior Arctic can exceed a factor of 3. Even with expected levels of error in the present derived FCD/FSD product, some constraints on the model can be considered at present with this method. A future comparison of results from the the IceSat2 and CryoSat-2 altimeters will provide insights into the relevance of measurement and statistical uncertainties, as will comparison of altimetrically derived floe chords measurements with visual imagery.

Even accounting for important caveats that arise from making satellite measurements, remotely sensing the sea ice FSD from altimeters at sub-daily resolutions can provide a significant increase in data for comparison and analysis of new sea ice models that parameterize the FSD. Previously the difficulty of making measurements of the FSD at relevant spatial and temporal scales has inhibited the wide-spread adoption of such floe-sensitive sea ice models. Understanding sea ice variability at the floe scale is also an important aspect of sea ice forecasting, and the ability to remotely assess the sea ice FSD at near-real-time will allow for further improvement of operational forecasting networks.

Data availability. CPOM sea ice data, including raw floe length data, are available on the CPOM data portal at http://www.cpom.ucl.ac.uk/csopr/seaice.htm The processed FCD/FSD statistics are available at https://github.com/chhorvat/CRYOSAT-FLOES/. The Roach et al. (2018a) FSTD model is publicly developed and available at https://github.com/lettie-roach/.

Appendix A: Proof that the FCD and FSD have the same statistical properties

For generic probability distributions $S(D)$ and $P(r)$, and a probability function $\tilde{F}(D;r)$, via equation 4 we have the relationship,

$$\langle D^n \rangle = \int_0^\infty dr\, P(r) \int_0^r D^n \tilde{F}(D;r)\, dD. \tag{A1}$$

Where we restrict the upper bounds on the second integral because $\tilde{F}(D;r)$ is zero for $D > r$. Under the scale-invariant sampling assumption $\tilde{F}(D;r)dD = G(\xi)d\xi$, where ~~$\xi = \frac{D}{r}$ for $D < r$~~ $\xi = \frac{D}{2r}$ for $D < 2r$ ($\xi < 1$). Therefore,

$$\langle D^n \rangle = \int_0^\infty dr\, P(r) \int_0^1 r^n \xi^n G(\xi)\, d\xi \tag{A2}$$

$$= \int_0^\infty dr\, P(r) r^n \int_0^1 \xi^n G(\xi) d\xi \tag{A3}$$

$$= A_n \cdot \langle r^n \rangle, \tag{A4}$$

where A_n is the n$^{\text{th}}$ moment of $G(\xi)$, a constant that depends on the functional form of G. For any such probability function (for example that derived in Sec. 2 for circular floes), the moments of the FSD and the moments of the FCD are proportional. Most of the hypothetical statistical distributions we would consider (for example, power laws) can be fully determined in terms of their moments, and thus the relationship between moments of the FSD and FCD is typically sufficient to reconstruct the underlying FSD.

Supposing $P(r)$ was a power-law function, converting Eq. 8 to an integral over ξ from 0 to 1, we have,

$$S(D) = \int_0^\infty \tilde{F}(D;r)P(r)dr = \int_0^1 \frac{P(D/\xi)G(\xi)}{\xi} \frac{P(D/2\xi)G(\xi)}{\xi} d\xi. \tag{A5}$$

For a power-law function, ~~$P(D/\xi) \propto \left(\frac{D}{\xi}\right)^{-\alpha}$~~ $P(D/(2\xi)) \propto \left(\frac{D}{\xi}\right)^{-\alpha}$ and

$$S(D) \propto \cdot D^{-\alpha} \int_0^1 \xi^{\alpha-1} G(\xi) d\xi = A_{\alpha-1} D^{-\alpha}. \tag{A6}$$

From Equations A4 and A6, and under the assumptions of Sec. 2, all moments of the FSD and FCD are related by a computable function of the moment only, and power-law FSDs are derived from power-law FCDs with the same scaling law. While the proportionality of moments and Eq. A6 prove that an observed power-law FCD must reflect an underlying power-law FSD, the same analysis used to arrive at Eq. A6 can be repeated to find $P(r)$ given a power-law distributed $S(D)$ as well.

Appendix B: Bounds on the Relationship between Chord Length and Floe Size Moments

The real altimetric data product has a finite sampling resolution D_{min} which can bias the computed FSD moments and power-law decay profile. For example, applied to real data with a finite sampling resolution , the integrals in equations 4 to 5 are taken beginning at the minimum observed chord lengths D_{min} and floe sizes $r_{min} = D_{min}/2$. Moments of the distributions S and P reflect only statistics for floes larger than D_{min} and r_{min}, respectively. All other aspects of this derivation remain the same, as ~~$F(r;D)$~~ $\tilde{F}(D;r)$ is zero for any $r < D/2$. However, the relationship expressed in Eq. 4 becomes:

$$\langle D^n \rangle = \int_{r_{min}}^\infty dr\, P(r) \frac{2^{n+1}}{\pi} r^n \int_{Y(r)}^{\frac{\pi}{2}} \sin(x)^n dx \tag{B1}$$

$$= A_n \langle r^n \rangle \left[1 - \frac{\int_{r_{min}}^\infty dr\, P(r) \frac{2^{n+1}}{\pi} r^n S_n(Y(r))}{A_n \langle r^n \rangle} \right] \tag{B2}$$

$$\equiv A_n \langle r^n \rangle \left[1 - E(P(r);n) \right]. \tag{B3}$$

where $Y(r) \equiv \sin^{-1}(\frac{D_{min}}{2r})$, $S_n(y) = \int_0^y sin^n(x)dx$, and E is the error in relating the n$^{\text{th}}$ moments of $S(D)$ and $P(r)$. Since $P(r)$ is unknown, E cannot be computed a priori. The function $S_n(Y(r))$ expresses the percentage of chords formed from

floes of size r that would be smaller than D_{min}, although it is not readily expressed as a function of n. The most pathological distributio is when $P(r)$ is a delta function at r_{min}, $P(r) = \delta(r - r_{min})$, $Y(r_{min}) = \pi/2$ and $E = 1$ as no chord lengths would be measured.

We can compute the error function for any delta function distribution as,

$$E(\delta(r - r^*); n) = \frac{S_n(Y(r^*))}{S_n(\frac{\pi}{2})}, \tag{B4}$$

and the misfit is the proportion of the integral of $\sin^n(x)$ betweeen 0 and $Y(r^*)$. Because $\sin(x)$ is monotonically increasing from $x = 0$ to $\pi/2$, the integral of S_n is bounded above:

$$S_n(Y(r^*)) \leq Y(r^*)\sin^n(Y(r^*)) = Y(r^*)\left(\frac{D_{min}}{2r^*}\right)^n, \tag{B5}$$

and the misfit error is bounded above by,

$$E(\delta(r - r^*; n)) \leq \left(\frac{D_{min}}{2r^*}\right)^n \frac{Y(r^*)}{\beta(\frac{n+1}{2}, \frac{1}{2})}. \tag{B6}$$

The reciprocal of the β function is equal to π at $n = 0$ and decreases sub-linearly, and so away from r_{min} the error term decays exponentially with n and is small even for nearly-pathological distributions (for n=1, $r^* = D_{min}$, for example, $E \leq \pi/24 \approx 14\%$. Knowing the distribution of errors behaves in this way allows us to establish upper bounds by integrating P as a sum of δ functions.

We note that increasing resolution of floe chords will result in tighter bounds on this error. When $Y(r)^* \leq 1$, which occurs when $r^* \geq \frac{D_{min}}{2\sin(1)} \approx 0.59 D_{min}$, we can exploit a tighter bound using the fact that $\sin^n(x) \leq x^n$,

$$S_n(Y(r^*)) \leq \frac{Y(r^*)^{n+1}}{n+1} \leq Y(r^*)\left(\frac{D_{min}}{2r^*}\right)^n. \tag{B7}$$

Using the same example as above ($n = 1$, $r^* = D_{min}$) bounds the error $E \leq \pi^2/144 \approx 7\%$. A real-world distribution of floe sizes must have a peak value above zero, thus by increasing the sampling resolution (say, for example, to near the size of pancakes, i.e. $D_{min} \approx 20$ meters or less, approached by the ICESAT-2 altimeter), this bound takes over and errors are reduced substantially.

We can explicitly solve Eq. B3 for distributions with power-law tails. These distributions are peaked at the minimum floe size, and so will have high moment error. For power laws with $\alpha = -1,\ -2,\ -3$, or -4, $E(P(r; \alpha, r_{min}), 1)$ is 1, 4, 16, or 25 percent. For $n = 2$, $E(P(r; \alpha, r_{min}), 2)$ is .003, .04, 2, or 9.6 percent: the increase in error with decreasing α is because sharper power law slopes concentrate most of the distribution towards the smallest scale.

Appendix C: Maximum Likelihood Estimation for Chord Length Distributions

Given a set of floe chords $\{D\}_i$ and an estimate of the beginning of a power-law tail D^*, we would like to find the most likely power-law floe size distribution $P(r; \alpha, r_{min})$ that generated them. As discussed in Appendix A, moments of the FSD and

FCD are related by a multiplicative factor, and the distributions themselves will share the same power-law exponent. Thus we may test the power-law hypothesis directly on the FCD $S(D)$. The power-law hypothesis means that $S(D)$ is of the form,

$$S(D) = \frac{(\alpha-1)}{D^*}\left(\frac{D}{D^*}\right)^{-\alpha}. \tag{C1}$$

Following (Muniruzzaman, 1957; Clauset et al., 2009) (see also the derivation in Stern et al. (2018a)), we compute the log-likelihood of the observations for a given α (eq. 10),

$$\mathcal{L} \equiv \ln \prod_{i=1}^{N} S(D_i) = \ln\left[\left(\frac{\alpha-1}{D^*}\right)^N \prod_{i=1}^{N}\left(\frac{D_i}{D^*}\right)^{-\alpha}\right] \tag{C2}$$

$$= N\ln(\alpha-1) + N(\alpha-1)\ln D^* - \alpha\sum_{i}^{N}\ln D_i. \tag{C3}$$

As the natural log is monotonically increasing in its argument, to find the most likely α, denoted $\hat{\alpha}$, we ~~solve a similar equation,~~ take the derivative with respect to α and set to zero,

$$\frac{1}{\alpha-1} + \ln(D^*) = \frac{1}{N}\sum_{i=1}^{N}\ln\frac{D_i}{D^*}. \tag{C4}$$

which resolves as a solution for the most likely α:

$$\hat{\alpha} = 1 + \frac{N}{\sum_{i=1}^{N}\ln\frac{D_i}{D^*}}. \tag{C5}$$

The above analysis concerns the most likely α that explains the FCD. ~~If the FCD has a power-law tail, then so will the FSD, and of the same exponent. However, we can also~~ We may ask a separate question: what is the most-likely ~~$\alpha = \alpha_P$ that explains~~ α, which we define as α_P, that would explain the FSD, given the explicit relationship that can be derived between $S(D)$ and a power-law distributed $P(r)$ examined in ~~Appendix A: $S(D) = C_\alpha P(r)$~~ Eq. 10:

$$S(D) = C\cdot B\left(\frac{1}{2},\frac{\alpha}{2}\right)\frac{2^{\alpha-1}}{\pi}D^{-\alpha} \tag{C6}$$

where C is unknown. Repeating the above analysis,

$$\mathcal{L} \equiv \ln\prod_{i=1}^{N} S(D_i) = \ln\left[C(\alpha_P)^N B\left(\frac{\alpha_P-1}{D^*}\frac{1}{2},\frac{\alpha_P}{2}\right)^N\left(\frac{2^{(\alpha_P-1)}}{\pi}\right)^N\prod_{i=1}^{N}\frac{D_i}{D^*}D_i^{-\alpha_P}\right] \tag{C7}$$

$$= N\ln C(\alpha_P) + N\ln(\alpha_P-1)B\left(\frac{1}{2},\frac{\alpha_P}{2}\right) + N(\alpha_P-1)\ln D^* 2 - N\ln\pi - \alpha_P\sum_{i}^{N}\ln D_i. \tag{C8}$$

Next ~~taking~~ we take the derivative of $\mathcal{L}$ with respect to α_P and setting to zero~~, we use the form of C_α identified in Appendix A for circular floes and the fact that $B'(x,y) = B(x,y)(\psi(x) - \psi(x+y))$~~. We use the fact that $B(x,y) = B(y,x)$, and $\frac{\partial B(x,y)}{\partial x} = B(x,y)(\psi(x) - \psi(x+y))$ where ψ is the digamma function, ~~therefore,~~ to find,

$$\frac{\partial \ln B\left(\frac{1}{2},\frac{\alpha_P}{2}\right)}{\partial\alpha_P} = \frac{1}{2}\left(\psi\left(\frac{\alpha_P}{2}\right) - \psi\left(\frac{\alpha_P+1}{2}\right)\right). \tag{C9}$$

The maximum likelihood ~~$\hat{\alpha}_P$~~ α_P is the solution to the transcendental equation,

$$\frac{1}{2}\left[\psi\left(\frac{\alpha_P}{2}\right)-\psi\left(\frac{\alpha_P+1}{2}\right)\right]+\frac{1}{\alpha_P-1}\ln 2=\frac{1}{N}\sum_{i=1}^{N}\frac{D_i}{D^*}\ln D_i. \tag{C10}$$

~~Although the decay coefficients for a FCD and FSD are the same, the most likely value $\hat{\alpha}$ that explains that data, and the most likely value $\hat{\alpha}_P$ that would explain the FSD that generated it are different, with $\hat{\alpha}_P > \hat{\alpha}$.~~

~~The derivation of $\hat{\alpha}_P$ is again a consequence of floe chords that can be generated from a floe of size r that lie below D^*. In practice, there is no *a priori* way to know the coefficients C_α upon which this derivation rests. The most effective technique is to compute $\hat{\alpha}$ according to C5 and perform hypothesis testing on that fit. If the power-law hypothesis is rejected for the FCD, it must be rejected for the FSD as well~~which is an alternative method for obtaining the FSD scaling.

Appendix D: Averaging and Segmenting FSD Statistics

Due to limitations in the number of floe chords recorded at any particular location over time, we do not include all geographic locations when computing hemispheric means. Averaging is performed by including only geographic regions where there are at least 25 recorded floe chords. The area being averaged over is thus not fixed in time. For seasonal cycle plots, we only include months which have enough measurements for all fully-sampled CryoSat-2 years (2011-2018). For annual averages, we include only those years where all CryoSat-2 months (excluding June-September) have enough measurements.

When masking additional regions to perform the model/observation comparisons in Fig. 6, we note that because the Roach et al. (2018a) model does not include processes that fragment larger floes into smaller floes in the absence of ocean surface waves, regions in the interior Arctic without wave activity have nearly all sea ice area belonging to the highest floe size categories. Nearly all regions where wave fracture is an active process also have ~~a~~ representative radii below about 10 km (Roach et al., 2019). We define regions that do not experience wave fracture as those with an abnormally high simulated representative radius, which we choose to be the 22$^{\text{nd}}$ floe size category ($\overline{r} = 18.6$ km) or above. The mask and comparisons in Fig. 6 are made by excluding all such areas.

Author contributions. CH derived the mathematical theory and wrote the manuscript. LR built and performed the climate model simulation. RT, AR, and AS provided and interpreted the CryoSat-2 data. KH, CG, CB, and BK contributed to the study design. All authors have participated in manuscript preparation.

Competing interests. The authors declare no competing interests.

Acknowledgements. CH was supported by the NOAA Climate and Global Change Postdoctoral Fellowship Program, administered by UCAR's Cooperative Programs for the Advancement of Earth System Science (CPAESS), sponsored in part through cooperative agreement number NA16NWS4620043, Years 2017–2021, with the National Oceanic and Atmospheric Administration (NOAA), U.S. Department of Commerce (DOC). CH, CG, and KH thank the American Mathematical Society for their support through the Math Research Community "Differential Equations, Probability, and Sea Ice", funded by NSF grants 1321794 and 1641020. LR was funded via Marsden contract VUW-1408 and the New Zealand Deep South National Science Challenge, MBIE contract number C01X1445. CMB was supported by the National Science Foundation grant PLR-1643431. BFK was supported by ONR grant N00014-17-1-2963 and NSF grant 1350795. RT, AR, and AS were supported by the UK NERC Centre for Polar Observation and Modelling and the European Space Agency

References

Alberello, A., Onorato, M., Bennetts, L., Vichi, M., Eayrs, C., MacHutchon, K., and Toffoli, A.: Brief communication: Pancake ice floe size distribution during the winter expansion of the Antarctic marginal ice zone, The Cryosphere, 13, 41–48, https://doi.org/10.5194/tc-13-41-2019, https://www.the-cryosphere-discuss.net/tc-2018-155/https://www.the-cryosphere.net/13/41/2019/, 2019.

Allard, R. A., Farrell, S. L., Hebert, D. A., Johnston, W. F., Li, L., Kurtz, N. T., Phelps, M. W., Posey, P. G., Tilling, R., Ridout, A., and Wallcraft, A. J.: Utilizing CryoSat-2 sea ice thickness to initialize a coupled ice-ocean modeling system, Journal of Geophysical Research: Oceans, 62, 1265–1280, https://doi.org/10.1016/j.asr.2017.12.030, https://linkinghub.elsevier.com/retrieve/pii/S0273117717309183, 2018.

Armitage, T. W. K. and Davidson, M. W. J.: Using the Interferometric Capabilities of the ESA CryoSat-2 Mission to Improve the Accuracy of Sea Ice Freeboard Retrievals, IEEE Transactions on Geoscience and Remote Sensing, 52, 529–536, https://doi.org/10.1109/TGRS.2013.2242082, http://ieeexplore.ieee.org/document/6479282/, 2014.

Armitage, T. W. K., Bacon, S., and Kwok, R.: Arctic Sea Level and Surface Circulation Response to the Arctic Oscillation, Geophysical Research Letters, 45, 6576–6584, https://doi.org/10.1029/2018GL078386, http://doi.wiley.com/10.1029/2018GL078386, 2018.

Batchelor, G. K.: The theory of homogeneous turbulence., Cambridge University Press, 1953.

Bateson, A. W., Feltham, D. L., Schröder, D., Hosekova, L., Ridley, J. K., and Aksenov, Y.: Impact of floe size distribution on seasonal fragmentation and melt of Arctic sea ice, The Cryosphere Discussions, pp. 1–35, https://doi.org/10.5194/tc-2019-44, https://www.the-cryosphere-discuss.net/tc-2019-44/, 2019.

Birnbaum, G. and Lüpkes, C.: A new parameterization of surface drag in the marginal sea ice zone, Tellus A, 54, 107–123, https://doi.org/10.1034/j.1600-0870.2002.00243.x, http://tellusa.net/index.php/tellusa/article/view/12121, 2002.

Clauset, A., Young, M., and Gleditsch, K. S.: On the Frequency of Severe Terrorist Events, Journal of Conflict Resolution, 51, 58–87, 2007.

Clauset, A., Shalizi, C. R., Newman, M. E. J., Rohilla Shalizi, C., and J Newman, M. E.: Power-Law Distributions in Empirical Data, SIAM Review, 51, 661–703, https://doi.org/10.1137/070710111, http://epubs.siam.org/doi/10.1137/070710111, 2009.

Day, J. J., Hawkins, E., and Tietsche, S.: Will Arctic sea ice thickness initialization improve seasonal forecast skill?, Geophysical Research Letters, 41, 7566–7575, https://doi.org/10.1002/2014GL061694, http://doi.wiley.com/10.1002/2014GL061694, 2014.

Feltham, D. L.: Sea Ice Rheology, Annual Review of Fluid Mechanics, 40, 91–112, https://doi.org/10.1146/annurev.fluid.40.111406.102151, http://www.annualreviews.org/doi/10.1146/annurev.fluid.40.111406.102151, 2008.

Gherardi, M. and Lagomarsino, M. C.: Characterizing the size and shape of sea ice floes, Sci. Rep, 5, 10 226, https://doi.org/10.1038/srep10226, http://www.nature.com/articles/srep10226, 2015.

Guerreiro, K., Fleury, S., Zakharova, E., Kouraev, A., Rémy, F., and Maisongrande, P.: Comparison of CryoSat-2 and ENVISAT radar freeboard over Arctic sea ice: Toward an improved Envisat freeboard retrieval, Cryosphere, 11, 2059–2073, https://doi.org/10.5194/tc-11-2059-2017, 2017.

Herman, A.: Molecular-dynamics simulation of clustering processes in sea-ice floes, Physical Review E - Statistical, Nonlinear, and Soft Matter Physics, 84, 1–11, https://doi.org/10.1103/PhysRevE.84.056104, 2011.

Herman, A., Evers, K.-U. U., and Reimer, N.: Floe-size distributions in laboratory ice broken by waves, Cryosphere, 12, 685–699, https://doi.org/10.5194/tc-12-685-2018, https://www.the-cryosphere-discuss.net/tc-2017-186/https://www.the-cryosphere.net/12/685/2018/, 2018.

Horvat, C. and Tziperman, E.: A prognostic model of the sea-ice floe size and thickness distribution, Cryosphere, 9, 2119–2134, https://doi.org/10.5194/tc-9-2119-2015, 2015.

Horvat, C. and Tziperman, E.: The evolution of scaling laws in the sea ice floe size distribution, Journal of Geophysical Research: Oceans, 122, 7630–7650, https://doi.org/10.1002/2016JC012573, http://doi.wiley.com/10.1002/2016JC012573, 2017.

Horvat, C. and Tziperman, E.: Understanding Melting due to Ocean Eddy Heat Fluxes at the Edge of Sea-Ice Floes, Geophysical Research Letters, 45, 9721–9730, https://doi.org/10.1029/2018GL079363, https://agupubs.onlinelibrary.wiley.com/doi/abs/10.1029/2018GL079363http://doi.wiley.com/10.1029/2018GL079363, 2018.

Hunke, E. C., Lipscomb, W. H., Turner, A. K., Jeffery, N., and Elliott, S.: CICE : the Los Alamos Sea Ice Model Documentation and Software User's Manual Version 5.1 LA-CC-06-012, Tech. rep., Los Alamos National Laboratory, http://oceans11.lanl.gov/trac/CICE, 2015.

Hwang, B., Wilkinson, J., Maksym, E., Graber, H. C., Schweiger, A., Horvat, C., Perovich, D. K., Arntsen, A. E., Stanton, T. P., Ren, J., Wadhams, P., Maksym, T., Graber, H. C., Schweiger, A., Horvat, C., Perovich, D. K., Arntsen, A. E., Timothy, P., Ren, J., and Wadhams, P.: Winter-to-summer transition of Arctic sea ice breakup and floe size distribution in the Beaufort Sea, Elementa: Science of the Anthropocene, 5, 40, https://doi.org/10.1525/elementa.232, http://www.elementascience.org/article/10.1525/elementa.232/, 2017.

JRA-55: JRA-55: Japanese 55-year Reanalysis, Daily 3-Hourly and 6-Hourly Data, Research Data Archive at the National Center for Atmospheric Research, Computational and Information Systems Laboratory, 2013.

Key, J.: Estimating the area fraction of geophysical fields from measurements along a transect, IEEE Transactions on Geoscience and Remote Sensing, 31, 1099–1102, https://doi.org/10.1109/36.263782, http://ieeexplore.ieee.org/document/263782/, 1993.

Key, J. and Peckham, S.: Probable errors in width distributions of sea ice leads measured along a transect, Journal of Geophysical Research, 96, 18 417, https://doi.org/10.1029/91JC01843, http://doi.wiley.com/10.1029/91JC01843, 1991.

Kobayashi, S., Ota, Y., Harada, Y., Ebita, A., Moriya, M., Onoda, H., Onogi, K., Kamahori, H., Kobayashi, C., Endo, H., Miyaoka, K., and Takahashi, K.: The JRA-55 Reanalysis: General Specifications and Basic Characteristics, Journal of the Meteorological Society of Japan. Ser. II, 93, 5–48, https://doi.org/10.2151/jmsj.2015-001, https://www.jstage.jst.go.jp/article/jmsj/93/1/93{_}2015-001/{_}article, 2015.

Kwok, R.: Arctic sea ice thickness, volume, and multiyear ice coverage: losses and coupled variability (1958–2018), Environmental Research Letters, 13, 105 005, https://doi.org/10.1088/1748-9326/aae3ec, http://stacks.iop.org/1748-9326/13/i=10/a=105005?key=crossref.33a163ccc3823012559fd268c096f877, 2018.

Laxon, S., Peacock, N., and Smith, D.: High interannual variability of sea ice thickness in the Arctic region, Nature, 425, 947–950, https://doi.org/10.1038/nature02050, http://www.nature.com/articles/nature02050, 2003.

Laxon, S. W., Giles, K. A., Ridout, A. L., Wingham, D. J., Willatt, R., Cullen, R., Kwok, R., Schweiger, A., Zhang, J., Haas, C., Hendricks, S., Krishfield, R., Kurtz, N., Farrell, S., and Davidson, M.: CryoSat-2 estimates of Arctic sea ice thickness and volume, Geophysical Research Letters, 40, 732–737, https://doi.org/10.1002/grl.50193, 2013.

Lindsay, R. W. and Rothrock, D. A.: Arctic sea ice leads from advanced very high resolution radiometer images, Journal of Geophysical Research, 100, 4533, https://doi.org/10.1029/94JC02393, http://dx.doi.org/10.1029/94JC02393http://doi.wiley.com/10.1029/94JC02393, 1995.

Lüpkes, C. and Birnbaum, G.: Surface drag in the Arctic marginal sea-ice zone: A comparison of different parameterisation concepts, Boundary-Layer Meteorology, 117, 179–211, https://doi.org/10.1007/s10546-005-1445-8, 2005.

Mandelbrot, B. B. and Wheeler, J. A.: The Fractal Geometry of Nature, vol. 51, W. H. Freeman, https://doi.org/10.1119/1.13295, http://aapt.scitation.org/doi/10.1119/1.13295, 1983.

Manucharyan, G. E. and Thompson, A. F.: Submesoscale Sea Ice-Ocean Interactions in Marginal Ice Zones, Journal of Geophysical Research: Oceans, 122, 9455–9475, https://doi.org/10.1002/2017JC012895, http://doi.wiley.com/10.1002/2017JC012895, 2017.

Muniruzzaman, A. N. M.: On Measures of Location and Dispersion and Tests of Hypotheses in a Pareto Population, Calcutta Statistical Association Bulletin, 7, 115–123, https://doi.org/10.1177/0008068319570303, http://journals.sagepub.com/doi/10.1177/0008068319570303, 1957.

Nere, N. K., Ramkrishna, D., Parker, B. E., Bell, W. V., and Mohan, P.: Transformation of the Chord-Length Distributions to Size Distributions for Nonspherical Particles with Orientation Bias †, Industrial & Engineering Chemistry Research, 46, 3041–3047, https://doi.org/10.1021/ie0609463, http://pubs.acs.org/doi/abs/10.1021/ie0609463, 2007.

Peacock, N. R. and Laxon, S. W.: Sea surface height determination in the Arctic Ocean from ERS altimetry, Journal of Geophysical Research C: Oceans, https://doi.org/10.1029/2001JC001026, 2004.

Perovich, D. K. and Jones, K. F.: The seasonal evolution of sea ice floe size distribution, J. Geophys. Res. Oceans, 119, 8767–8777, https://doi.org/10.1002/2014JC010136, http://doi.wiley.com/10.1002/2014JC010136, 2014.

Pons, M.-N., Milferstedt, K., and Morgenroth, E.: Modeling of chord length distributions, Chemical Engineering Science, 61, 3962–3973, https://doi.org/10.1016/j.ces.2006.01.036, http://linkinghub.elsevier.com/retrieve/pii/S0009250906000881, 2006.

Quartly, G. D., Rinne, E., Passaro, M., Andersen, O. B., Dinardo, S., Fleury, S., Guillot, A., Hendricks, S., Kurekin, A. A., Müller, F. L., Ricker, R., Skourup, H., and Tsamados, M.: Retrieving Sea Level and Freeboard in the Arctic: A Review of Current Radar Altimetry Methodologies and Future Perspectives, Remote Sensing, 11, 881, https://doi.org/10.3390/rs11070881, https://www.mdpi.com/2072-4292/11/7/881, 2019.

Roach, L., Bitz, C., Horvat, C., and Dean, S.: Advances in modelling interactions between sea ice and ocean surface waves, Journal of Advances in Modeling Earth Systems (in review), pp. 1–14, 2019.

Roach, L. A., Horvat, C., Dean, S. M., and Bitz, C. M.: An emergent sea ice floe size distribution in a global coupled ocean–sea ice model, Journal of Geophysical Research: Oceans, 123, 4322–4337, https://doi.org/10.1029/2017JC013692, http://doi.wiley.com/10.1029/2017JC013692, 2018a.

Roach, L. A., Smith, M. M., and Dean, S. M.: Quantifying growth of pancake sea ice floes using images from drifting buoys, Journal of Geophysical Research: Oceans, 123, 2851–2866, https://doi.org/10.1002/2017JC013693, http://doi.wiley.com/10.1002/2017JC013693, 2018b.

Roberts, A. F., Hunke, E. C., Kamal, S. M., Lipscomb, W. H., Horvat, C., and Maslowski, W.: A Variational Method for Sea Ice Ridging in Earth System Models, Journal of Advances in Modeling Earth Systems, p. 2018MS001395, https://doi.org/10.1029/2018MS001395, http://doi.wiley.com/10.1029/2018MS001395https://onlinelibrary.wiley.com/doi/abs/10.1029/2018MS001395, 2019.

Rothrock, D. A. and Thorndike, A. S.: Measuring the Sea Ice Floe Size Distribution., Journal of Geophysical Research, 89, 6477–6486, https://doi.org/10.1029/JC089iC04p06477, 1984a.

Rothrock, D. A. and Thorndike, A. S.: Measuring the sea-ice floe size distribution, J. Geophys. Res., 89, 6477–6486, 1984b.

Rynders, S., Aksenov, Y., Feltham, D., Nurser, G., and Naveira Garabato, A.: Modelling MIZ dynamics in a global model, in: EGU General Assembly Conference Abstracts, p. 1004, 2016.

Sandberg Sorensen, L., Simonsen, S., Langley, K., Gray, L., Helm, V., Nilsson, J., Stenseng, L., Skourup, H., Forsberg, R., and Davidson, M.: Validation of CryoSat-2 SARIn Data over Austfonna Ice Cap Using Airborne Laser Scanner Measurements, Remote Sensing, 10, 1354, https://doi.org/10.3390/rs10091354, http://www.mdpi.com/2072-4292/10/9/1354, 2018.

Schröder, D., Feltham, D. L., Tsamados, M., Ridout, A., and Tilling, R.: New insight from CryoSat-2 sea ice thickness for sea ice modelling, The Cryosphere Discussions, 1, 1–25, https://doi.org/10.5194/tc-2018-159, https://www.the-cryosphere-discuss.net/tc-2018-159/, 2018.

Schulson, E. M. and Hibler, W. D.: The fracture of ice on scales large and small: Arctic leads and wing cracks, Journal of Glaciology, 37, 319–322, https://doi.org/10.1017/S0022143000005748, https://www.cambridge.org/core/product/identifier/S0022143000005748/type/journal{_}article, 1991.

Skourup, H., Simonsen, S. B., Sorensen, L., Bella, A., Forsberg, R., Hvidegaard, S., and Helm, V.: ESA CryoVEx/EU ICE-ARC 2016—Airborne Field Campaign with ASIRAS Radar and Laser Scanner over Austfonna, Fram Strait and the Wandel Sea, Tech. rep., National Space Institute, Technical University of Denmark, 2017.

Smith, M. and Thomson, J.: Scaling observations of surface waves in the Beaufort Sea, Elementa: Science of the Anthropocene, 4, 000 097, https://doi.org/10.12952/journal.elementa.000097, http://www.elementascience.org/articles/10.12952/journal.elementa.000097, 2016.

Squire, V. A.: Of ocean waves and sea-ice revisited, Cold Regions Science and Technology, 49, 110–133, https://doi.org/10.1016/j.coldregions.2007.04.007, 2007.

Squire, V. A., Dugan, J. P., Wadhams, P., Rottier, P. J., and Liu, a. K.: Of Ocean Waves and Sea Ice, Annual Review of Fluid Mechanics, 27, 115–168, https://doi.org/10.1146/annurev.fl.27.010195.000555, http://www.annualreviews.org/doi/abs/10.1146/annurev.fl.27.010195.000555http://www.annualreviews.org/doi/10.1146/annurev.fl.27.010195.000555, 1995.

Steele, M.: Sea ice melting and floe geometry in a simple ice-ocean model, Journal of Geophysical Research: Oceans, 97, 17 729–17 738, https://doi.org/10.1029/92JC01755, http://doi.wiley.com/10.1029/92JC01755, 1992.

Steer, A., Worby, A., and Heil, P.: Observed changes in sea-ice floe size distribution during early summer in the western Weddell Sea, Deep Sea Research Part II: Topical Studies in Oceanography, 55, 933–942, https://doi.org/10.1016/j.dsr2.2007.12.016, http://www.sciencedirect.com/science/article/pii/S0967064508000362, 2008.

Stern, H. L., Schweiger, A. J., Stark, M., Zhang, J., Steele, M., and Hwang, B.: Seasonal evolution of the sea-ice floe size distribution in the Beaufort and Chukchi seas, Elementa: Science of the Anthropocene, 6, 48, https://doi.org/10.1525/elementa.304, https://www.elementascience.org/article/10.1525/elementa.305/https://www.elementascience.org/article/10.1525/elementa.304/, 2018a.

Stern, H. L., Schweiger, A. J., Zhang, J., and Steele, M.: On reconciling disparate studies of the sea-ice floe size distribution, Elem Sci Anth, 6, 49, https://doi.org/10.1525/elementa.304, https://www.elementascience.org/article/10.1525/elementa.304/, 2018b.

Tilling, R., Ridout, A., and Shepherd, A.: Assessing the impact of geometric sampling differences on Arctic sea ice thickness from Envisat and CryoSat-2, in: Abstract C11A-0341 presented at 2018 Fall Meeting, AGU, Washington, D.C., 10-14 Dec., 2018a.

Tilling, R., Ridout, A., and Shepherd, A.: Assessing the impact of lead and floe sampling on Arctic sea ice thickness estimates from Envisat and CryoSat-2, Submitted to: Advances in Space Research, 2019.

Tilling, R. L., Ridout, A., and Shepherd, A.: Near-real-time Arctic sea ice thickness and volume from CryoSat-2, Cryosphere, https://doi.org/10.5194/tc-10-2003-2016, 2016.

Tilling, R. L., Ridout, A., and Shepherd, A.: Estimating Arctic sea ice thickness and volume using CryoSat-2 radar altimeter data, Advances in Space Research, https://doi.org/10.1016/j.asr.2017.10.051, 2018b.

Tolman, H. L. H. L.: User manual and system documentation of WAVEWATCH III TM version 3.14, Technical Note 276, 276, 194, ftp://ftp.ifremer.fr/ifremer/cersat/products/gridded/wavewatch3/HINDCAST/publications/Tolman{_}etal{_}MMAB276{_}2009.pdf{%}0Apapers3://publication/uuid/E1C39B58-DBCB-4F8A-ADCD-F2D2210DDC46, 2009.

Toyota, T., Takatsuji, S., and Nakayama, M.: Characteristics of sea ice floe size distribution in the seasonal ice zone, Geophys. Res. Lett., 33, L02 616, https://doi.org/10.1029/2005GL024556, http://dx.doi.org/10.1029/2005GL024556, 2006.

Toyota, T., Haas, C., and Tamura, T.: Size distribution and shape properties of relatively small sea-ice floes in the Antarctic marginal ice zone in late winter, Deep-Sea Research Part II: Topical Studies in Oceanography, 58, 1182–1193, https://doi.org/10.1016/j.dsr2.2010.10.034, 2011.

Toyota, T., Kohout, A., and Fraser, A. D.: Formation processes of sea ice floe size distribution in the interior pack and its relationship to the marginal ice zone off East Antarctica, Deep Sea Res. Pt II, 131, 28–40, https://doi.org/10.1016/j.dsr2.2015.10.003, http://www.sciencedirect.com/science/article/pii/S0967064515003252http://dx.doi.org/10.1016/j.dsr2.2015.10.003, 2016.

Tsamados, M., Feltham, D. L., Schroeder, D., Flocco, D., Farrell, S. L., Kurtz, N., Laxon, S. W., and Bacon, S.: Impact of Variable Atmospheric and Oceanic Form Drag on Simulations of Arctic Sea Ice*, Journal of Physical Oceanography, 44, 1329–1353, https://doi.org/10.1175/JPO-D-13-0215.1, 2014.

Virkar, Y. and Clauset, A.: Power-law distributions in binned empirical data, The Annals of Applied Statistics, 8, 89–119, https://doi.org/10.1214/13-AOAS710, http://projecteuclid.org/euclid.aoas/1396966280, 2014.

Wadhams, P., Squire, V. a., Goodman, D. J., Cowan, A. M., and Moore, S. C.: The attenuation rates of ocean waves in the marginal ice zone, Journal of Geophysical Research, 93, 6799, https://doi.org/10.1029/JC093iC06p06799, http://doi.wiley.com/10.1029/JC093iC06p06799, 1988.

Wernecke, A. and Kaleschke, L.: Lead detection in Arctic sea ice from CryoSat-2: Quality assessment, lead area fraction and width distribution, Cryosphere, 9, 1955–1968, https://doi.org/10.5194/tc-9-1955-2015, 2015.

Wilchinsky, A. V. and Feltham, D. L.: Modelling the rheology of sea ice as a collection of diamond-shaped floes, Journal of Non-Newtonian Fluid Mechanics, 138, 22–32, https://doi.org/10.1016/j.jnnfm.2006.05.001, 2006.

Wilchinsky, A. V. and Feltham, D. L.: Modeling Coulombic failure of sea ice with leads, Journal of Geophysical Research: Oceans, 116, C08 040, https://doi.org/10.1029/2011JC007071, 2011.

Williams, T. D., Bennetts, L. G., Squire, V. A., Dumont, D., and Bertino, L.: Wave-ice interactions in the marginal ice zone. Part 1: Theoretical foundations, Ocean Modelling, 71, 81–91, https://doi.org/10.1016/j.ocemod.2013.05.010, 2013.

Zhang, J., Schweiger, A., Steele, M., and Stern, H.: Sea ice floe size distribution in the marginal ice zone: Theory and numerical experiments, J. Geophys. Res. Oceans, 120, 3484–3498, https://doi.org/10.1002/2015JC010770, http://doi.wiley.com/10.1002/2015JC010770, 2015.

Zhang, J., Stern, H., Hwang, B., Schweiger, A., Steele, M., Stark, M., and Graber, H. C.: Modeling the seasonal evolution of the Arctic sea ice floe size distribution, Elementa, 4, 000 126, https://doi.org/10.12952/journal.elementa.000126, http://elementascience.org/article/info:doi/10.12952/journal.elementa.000126, 2016.